SANDIA REPORT

Compact Wire Array Sources: Power Scaling and Implosion Physics

Brent Jones, Michael E. Cuneo, David J. Ampleford, Christine A. Coverdale, Eduardo M. Waisman, Roger A. Vesey, Jason D. Serrano, Marcelino P. Vigil, Michael C. Jones, Andrey A. Esaulov, Victor L. Kantsyrev, Alla S. Safronova, Vladimir V. Ivanov, Alexandre S. Chuvatin, Leonid I. Rudakov

Sandia National Laboratories

Compact Wire Array Sources:
Power Scaling and Implosion Physics

B. Jones
Z Experiments

M.E. Cuneo
Z Experiments

D.J. Ampleford
Z Experiments

C.A. Coverdale
Systems Technologies

E.M. Waisman
Z Experiments

R.A. Vesey
ICF Target Design

J.D. Serrano
Radiation Effects Research

M.P. Vigil
Z Diagnostics

M.C. Jones
Z Diagnostics

Sandia National Laboratories
P.O. Box 5800
Albuquerque, NM 87185

A.A. Esaulov
Department of Physics

V.L. Kantsyrev
Department of Physics

A.S. Safronova
Department of Physics

V.V. Ivanov
Department of Physics

University of Nevada, Reno
Reno, NV 89557

A.S. Chuvatin

Laboratoire de Physique et Technologie des Plasmas
Laboratoire du Centre National
de la Recherche Scientifique
Ecole Polytechnique
91128 Palaiseau, France

L.I. Rudakov

Icarus Research
P.O. Box 30780
Bethesda, MD 20824-0780

Abstract

A series of ten shots were performed on the Saturn generator in short pulse mode in order to study planar and small-diameter cylindrical tungsten wire arrays at $\sim$5 MA current levels and 50-60 ns implosion times as candidates for compact z-pinch radiation sources. A new vacuum hohlraum configuration has been proposed in which multiple z pinches are driven in parallel by a pulsed power generator. Each pinch resides in a separate return current cage, serving also as a primary hohlraum. A collection of such radiation sources surround a compact secondary hohlraum, which may potentially provide an attractive Planckian radiation source or house an inertial confinement fusion fuel capsule. Prior to studying this concept experimentally or numerically, advanced compact wire array loads must be developed and their scaling behavior understood. The 2008 Saturn planar array experiments extend the data set presented in Ref. [1], which studied planar arrays at $\sim$3 MA, 100 ns in Saturn long pulse mode. Planar wire array power and yield scaling studies now include current levels directly applicable to multi-pinch experiments that could be performed on the 25 MA Z machine. A maximum total x-ray power of 15 TW (250 kJ in the main pulse, 330 kJ total yield) was observed with a 12-mm-wide planar array at 5.3 MA, 52 ns. The full data set indicates power scaling that is sub-quadratic with load current, while total and main pulse yields are closer to quadratic; these trends are similar to observations of compact cylindrical tungsten arrays on Z. We continue the investigation of energy coupling in these short pulse Saturn experiments using zero-dimensional-type implosion modeling and pinhole imaging, indicating 16 cm/μs implosion velocity in a 12-mm-wide array. The same phenomena of significant trailing mass and evidence for resistive heating are observed at 5 MA as at 3 MA. 17 kJ of Al K-shell radiation was obtained in one Al planar array fielded at 5.5 MA, 57 ns and we compare this to cylindrical array results in the context of a K-shell yield scaling model. We have also performed an initial study of compact 3 mm diameter cylindrical wire arrays, which are alternate candidates for a multi-pinch vacuum hohlraum concept. These massive 3.4 and 6 mg/cm loads may have been impacted by opacity, producing a maximum x-ray power of 7 TW at 4.5 MA, 45 ns. Future research directions in compact x-ray sources are discussed.

Acknowledgment

Contents

List of Figures

List of Tables

Chapter 1

Introduction

Wire array z pinches are intense and efficient soft x-ray sources, producing up to 200 TW and 1.8 MJ of radiation [2] on Sandia's Z machine [3]. Z-pinch loads are used for a variety of high energy density physics applications, including inertial confinement fusion (ICF) studies, K-shell x-ray generation for radiation effects research, and radiation and atomic physics [4].

The double-ended vacuum hohlraum z-pinch-driven ICF concept [5] which has been extensively studied on the Z machine [6] relies on a cylindrical primary hohlraum which also serves as the return current canister for the z-pinch radiation source on axis. The surface area of the hohlraum is thus constrained by the initial geometry of the cylindrical wire array. For a fixed x-ray pulse shape, the peak radiated power required to produce a given hohlraum temperature is roughly proportional to the hohlraum surface area [7]. The hohlraum temperature requirement is typically fixed by the design of the fuel capsule which resides in a secondary hohlraum driven from either end by two z-pinch-driven primaries. Thus, reducing the hohlraum area is attractive for reducing the power requirement placed on the z-pinch radiation source. This path requires advanced wire array development in order to achieve suitably high x-ray power from a compact load. In this report, we discuss experiments studying planar [8] and small-diameter cylindrical wire arrays [9] as candidates for a compact soft x-ray source.

A new z-pinch-driven hohlraum architecture has been proposed (L. I. Rudakov) in which multiple z-pinch radiation sources are driven in parallel by the pulsed power generator (i.e. the total load current is split between several compact wire arrays). An example of this configuration is shown in Fig. 1.1(a), in which four planar wire arrays surround a central secondary hohlraum. These arrays are each imploded in magnetically isolated return current cages that also serve as the primary hohlraum walls. Such a vacuum hohlraum configuration provides large static volumes affording good characterization of the hohlraum energetics. The secondary hohlraum could be used for ICF capsule drive as shown, or to produce more intense Planckian x-ray sources than the standard z-pinch-driven vacuum hohlraum. Driving multiple loads in parallel would present a reduced inductance to the generator, and could allow higher achievable total load current to be coupled.

Both the double-ended vacuum hohlraum and the multi-pinch version of Fig. 1.1
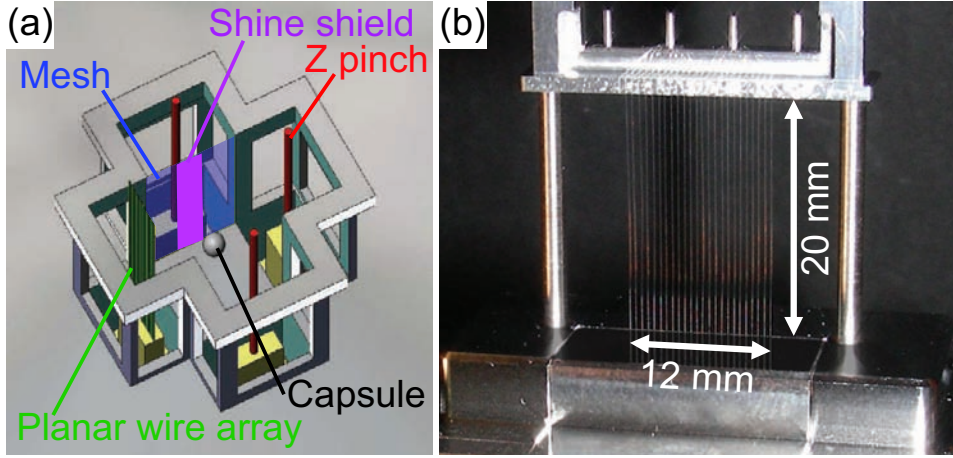
Figure 1.1. (a) A new concept for z-pinch driven vacuum hohlraum experiments (L.I. Rudakov) is to surround a central secondary hohlraum by multiple wire array radiation sources driven in parallel by the generator. Four planar wire array sources are shown in this example, each in a magnetically isolated return current structure serving also as a primary hohlraum. An ICF capsule is shown in the center of the configuration, but the concept may also be attractive for producing compact Planckian radiation sources. Since the generator current is split between the multiple loads, planar wire array studies on Saturn can be directly relevant to this multi-pinch concept on Z. (b) A photograph of a 12-mm-width, 24-wire, 2 mg/cm planar wire array shot on Saturn in August 2008.

would benefit from the development of compact wire array sources capable of driving primary hohlraums with low surface area. The multi-pinch concept has the additional advantage that the performance of each individual wire array load can be assessed on a smaller pulsed power driver before designing coupled experiments on a larger facility. Thus, work done to establish power and yield scaling using a single load on Saturn can be directly applied to assess multi-pinch concepts on Z. Here we have shown four planar wire arrays driving the secondary hohlraum, but the concept is more general; a variable number of parallel loads could be included, and these could be planar, ultra-compact cylindrical, or any number of other wire array load configurations. In the present work, we build on Ref. [1] continuing to assess planar wire arrays at 8-20 mm widths, and also perform initial experiments with 3 mm diameter cylindrical wire arrays at multi-MA levels.

The reduction of the wire array area from a cylindrical to a planar geometry may allow for a significant reduction in primary hohlraum area (the area of a rectangular current return electrode), as one dimension can be as thin as twice the anode-cathode feed gap width and no longer has to be wider than the array diameter. This advantage

assumes that planar wire arrays retain their relatively fast rise times and high powers as they are scaled up to higher drive currents, which is a prime motivation for the experiments on Saturn discussed in this report. We note that planar arrays are not required to outperform cylindrical wire arrays–if there is in fact a reduction in x-ray power, this might be offset by the potential reduction in primary hohlraum area. Ultimately, x-ray power scaling experiments must be complemented by integrated hohlraum and capsule modeling in order to determine whether planar-array-driven hohlraum energetics competes with the use of compact cylindrical wire array sources (e.g. the standard double-ended vacuum hohlraum).

Recently, planar wire array configurations, in which the wires are arranged as a linear array confining the mass within a plane, have attracted attention in the z-pinch community. Experiments on the 1 MA Zebra generator [10] at the University of Nevada, Reno, produced implosions with < 10 ns x-ray rise times and powers as high as 0.34 TW/cm, comparable to the most powerful cylindrical wire array implosions studied at that facility [8]. This behavior is surprising, as the standard intuition regarding cylindrical arrays is that high implosion velocity and a radially narrow plasma shell are required to achieve a fast rising and high power x-ray pulse. The planar array distributes the initial mass profile radially, which is not intuitively optimal for providing high implosion velocity. Numerical modeling [11, 12] and laser shadowgraphy measurements [13] indicate, however, that the wires implode in a cascade, with magnetic Rayleigh-Taylor implosion instabilities being stabilized to some extent as the implosion front impacts each adjacent wire on its way toward the axis. This suggests that a linear array mitigates instabilities in a manner analogous to a multiply nested wire array; nested cylindrical wire arrays have been previously demonstrated to enhance the radiated x-ray power and shorten the pulse due to mitigation of the magnetic Rayleigh-Taylor (MRT) implosion instability [2] as the current is switched from the outer to the inner array during the implosion [14]. It is not obvious whether the detrimental lower implosion velocity or the beneficial MRT snowplow stabilization will dominate the planar array dynamics. Experimentation is required to assess achievable x-ray powers from multi-MA planar wire array loads.

Previous publications have also discussed the possibility of enhanced Ohmic heating due to Hall resistivity effects in wire array z pinches, suggesting that the effect might be exaggerated and thus more clearly observable in planar arrays versus cylindrical arrays due to a smaller amount of coupled kinetic energy in the planar array case [15, 8]. Numerical modeling of wire arrays with a three-dimensional (3D) magnetohydrodynamic (MHD) code has indicated that resistive heating can play a role in cylindrical wire array energy deposition, but this contribution has been thought to be strongest and dominant only after the main x-ray peak [16]. These simulations assumed Spitzer resistivity, however, and would not have reflected the effects of enhanced resistivity due to Hall physics if in fact this phenomenon occurs and is significant in modifying the pinch energetics. If planar arrays offer an opportunity to assess the role of Ohmic heating in wire array plasmas, this insight would be generally beneficial to our understanding of z-pinch physics.

Planar arrays are thus interesting objects from a z-pinch physics perspective, and their study may shed light on instability mitigation and plasma heating mechanisms. Beyond basic physics issues, these arrays may be particularly attractive for ICF research due to the reduced volume occupied by the initial load configuration.

A final motivating factor in studying planar arrays is the report from the GIT-12 generator (4.7 MA, 1.7 μs implosion time) of an increase in Al K-shell yield by a factor of $\sim$2 compared to previous cylindrical arrays studied [17]. Wire arrays for producing K-shell x-rays are typically larger diameter than the compact ICF loads, placing the mass at large initial diameter so that high implosion velocities and thus plasma temperatures can be achieved for ionizing to the K shell [18]. It is arguably even less intuitive that planar wire arrays would benefit K-shell x-ray production, as the mass is radially distributed rather than initiated at large diameter, but this is another topic that can be addressed on Saturn.

Highly compact cylindrical arrays may provide an alternate load configuration for driving a multi-pinch hohlraum concept as in Fig. 1.1(a). Initial studies of 6 mm diameter Al wire arrays at 1 MA on the Zebra generator indicated comparable performance to planar Al arrays and higher x-ray power and yield than for 8-16 mm diameter Al cylindrical arrays [8]. A recent systematic study of cylindrical arrays from 1-16 mm diameter on Zebra indicates highest achievable x-ray power for 3-8 mm array diameters [9]. Arrays of 1-2 mm diameter exhibited a significant drop in peak x-ray power, as well as multiple x-ray peaks often characteristic of non-kinetic radiation sources such as single wires and x-pinches. The smallest diameter arrays, including those at 3 mm, couple reduced kinetic energy from the generator, and similarly to planar wire arrays there is significant evidence for resistive heating and trailing mass playing important roles in the dynamics [9]. If the x-ray power and yield of an ultra-compact cylindrical wire array scales favorably to $\sim$5 MA current levels, then this load configuration might also be attractive for the multi-pinch vacuum hohlraum concept discussed above. At multi-MA currents, these loads will be quite massive (even more so than planar wire arrays) and opacity could begin limiting the x-ray power.

The following section describes the shot plan and experimental goals for the August 2008 Saturn compact wire array series. The third chapter presents the experimental results, including tungsten power and yield scaling experiments, compact array dynamics and energetics analysis, and Al K-shell x-ray production from 3-5 MA planar wire arrays. A concluding chapter summarizes the results and discusses possible future experiments and numerical design studies related to compact wire array sources and the multi-pinch vacuum hohlraum concept. Primary goals in this report are to provide fairly complete documentation of the experiments in order to facilitate ongoing collaborations, to outline near-term analysis goals, to establish multi-MA scaling for planar wire arrays in order to support design studies of multi-pinch concepts for the Z machine, and to discuss future directions for study of compact wire arrays.

Chapter 2

Compact Wire Array Experiment Design

The two primary goals in the August 2008 experimental campaign were to complete the data set of Saturn tungsten planar wire arrays by extending the load current to ~5 MA, and to collect initial data for 3 mm diameter cylindrical wire arrays at multi-MA levels.

For the May-June 2007 planar wire array series, Saturn was operated in long pulse mode in order to access 100 ns implosion times. This allowed for a more direct comparison with Zebra data [8], and at implosion times directly relevant to the Z machine. However, this is shorter than the natural rise time of the Saturn generator in this mode, and so the arrays were imploding when the load current had reached only ~3 MA. We were not able to access current levels that are directly relevant to a multi-pinch vacuum hohlraum concept such as in Fig. 1.1(a). Thus, Saturn was run in short pulse mode for August 2008 experiments in order to access higher load currents. As will be discussed, zero-dimensional (0D) type implosion simulation with a coupled circuit model performed pre-shot during the experimental design phase predicted 4-5 MA for the identical planar array load hardware as in 2007 but with the machine in short instead of long pulse mode. This used a conservative estimate of the flow impedance, and recent empirical evidence [19] suggested that the 6 inch convolute (used in August 2008) should exhibit less flow loss than the 12 inch convolute (used in May-June 2007) when in short pulse mode. In fact we obtained 5-6 MA in the 2008 planar array experiments. The Saturn short-pulse mode [20] typically exhibits a peak in the load current waveform at < 60 ns, and so while are able to access higher current, the implosion times are now significantly shorter than on Zebra or Z. However, the final data set extends over significant ranges of current, implosion time, and array width, and so we are able to extract fairly solid conclusions about power and yield scaling of multi-MA planar wire arrays as will be discussed.

For consistency between experiments, to reduce cost, and to expedite load design, the planar array hardware style was nearly identical to the May-June 2007 experiments. Drawings and detailed description of this hardware is found in Ref. [1]. The large AK gaps were retained, though it remains highly desirable in future experiments to reduce AK gaps in order to reduce inductance and increase load current, and also to

Table 2.1. Planar and compact cylindrical wire array design parameters from the August 2008 Saturn shot series. Table 2.2 lists calculated implosion times, load currents, and coupled energies, while Tables 3.1 and 3.2 list experimental results.

Shot number	Wire material	Array height, h (mm)	Array width, W (mm)	Wire number	Wire diameter (μm)	Array mass (mg/cm)	Design implosion time
3744	W	20	8	16	40.60	3.987	Nominal
3745	W	20	12	24	23.50	2.004	Nominal
3746	W	20	12	24	23.50	2.004	Nominal
3747	W	20	8	16	40.60	3.987	Nominal
3748	Al 5056	20	20	40	30.50	0.789	Nominal
3752	W	20	20	40	11.43	0.790	Nominal
Shot number	Wire material	Array height, h (mm)	Array diameter (mm)	Wire number	Wire diameter (μm)	Array mass (mg/cm)	Design implosion time
3753	W	20	3	24	40.60	5.981	Early
3754	W	20	3	24	30.50	3.375	Earlier
3755	W	20	3	24	40.60	5.981	Early
3756	W	20	3	24	30.50	3.375	Earlier

reduce primary hohlraum surface area. The return current cage and diagnostic access was identical in 2007-2008. Interwire gap near 0.5 mm was again chosen for all planar wire arrays in 2008 for consistency, but investigation of smaller interwire gaps would be interesting. Changes to the 2008 hardware included matching the inner MITLs to the 6 inch convolute instead of the 12 inch convolute, and four (0°, 90°, 180°, 270°) instead of two (0°, 180°) load B-dots.

These experiments were designed to determine the scaling of peak x-ray power and x-ray energy in the main pulse of planar arrays for application to the multi-pinch vacuum hohlraum concept. The critical scalings are (1) with implosion time at constant array width (this is a mass scan), (2) with array width at fixed implosion time, and (3) with peak drive current at constant implosion time and width. Saturn data from May-June 2007 were used to evaluate (1) and (2). Issue (3) is evaluated using data both from Saturn (May-June 2007 at ∼3 MA and now August 2008 data at 5-6 MA) and from the University of Nevada, Reno, Zebra generator at 1 MA. We will also present multivariate fitting to the full planar array data set in order to infer dependence of x-ray power and yield on load current, width, and implosion time.

The second goal of the August 2008 shot series was to study ultra-compact cylindrical wire arrays. As mentioned earlier, work on Zebra has suggested that 3 mm diameters may be the smallest possible for retaining reasonable x-ray power in a well-defined

single peak. Thus, this diameter was chosen for initial Saturn experiments. The machine was also operated in short pulse mode for these experiments. This provided less machine turnaround time and greater shot rate, but perhaps more importantly allowed higher currents to be accessed and with loads at lower masses than in Saturn long pulse mode. As will be discussed, these highly compact arrays were still quite massive, and so there are concerns with opacity limiting the radiated power achieved. Large AK gaps were employed to provide insensitivity to alignment, and to allow 4-mm-wide diagnostic access slots in the return current canister so that the full initial diameter of the wire array can be viewed allowing for 0.5 mm of hole closure per side. Figure 2.1 shows a drawing of the load hardware region, and a view along the 35° diagnostic line of sight (views are essentially identical from LOS A, B, and C).

Ten shots were planned and executed on Saturn during August 2008. The load parameters for this series are specified in Table 2.1. Shots 3744-3747 and 3752 were tungsten planar arrays fielded at the widths studied previously at ∼3 MA. The current is increased to ∼5 MA for these short pulse shots, and these are used to investigate power and yield scaling to higher currents more directly relevant for potential Z experiments fielding multiple planar arrays in parallel. One Al planar array shot, 3748, will study how effective planar wire arrays are at producing K-shell x-rays at 5 MA current and will complement shot 3688 at 3 MA. Four shots, 3753-3756, were
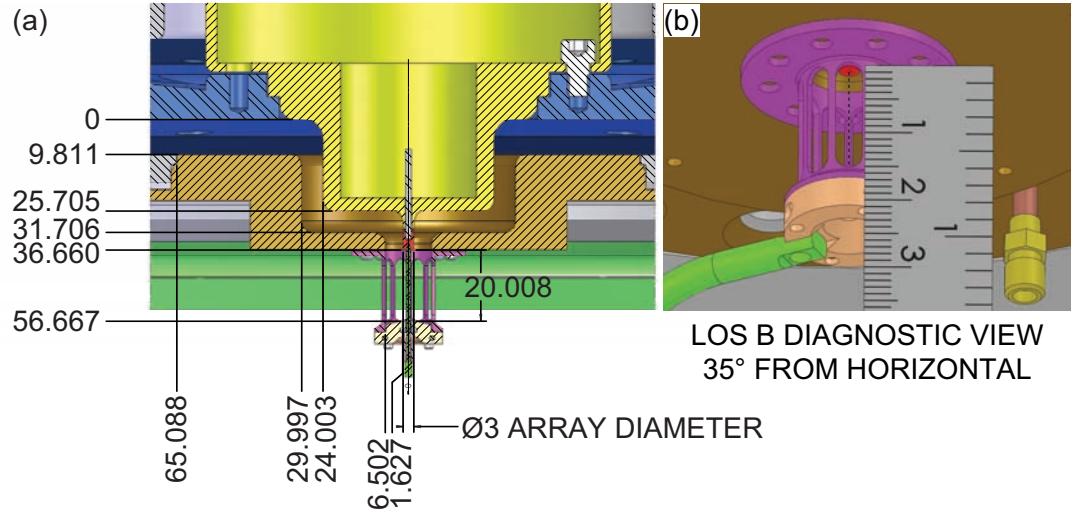
Figure 2.1. Drawing of the load region for the hardware design used in the August 2008 compact cylindrical wire array Saturn experiments. Dimensions are in millimeters. (b) Orthographic view of the load region at 35° below the horizontal from LOS A, B, or C. The viewable z-pinch axis is indicated by a dashed line. The centimeter-scale rule is shown in the plane perpendicular to the viewing line of sight. Courtesy of M. Vigil (1675).

fielded to provide preliminary data on ultra-compact 3 mm diameter cylindrical wire arrays at two masses to determine how x-ray power and yield scale from results at 1 MA on Zebra. For all of these shots, a series of electrical and x-ray power, yield and imaging diagnostics were fielded as described below to study the planar array implosion dynamics and energy coupling.

Pre-shot 0D-type modeling for load design

The load widths and implosion times were chosen to meet experimental goals as discussed above. With the inter-wire gap also fixed, the remaining as-yet-unspecified design parameter is the wire size. This must be chosen to give the array the appropriate mass so that the appropriate implosion time will be achieved when coupled to the generator. In the case of cylindrical wire arrays, 0D thin-shell calculations are typically employed in load design calculations to choose the load mass [21]. Here, the wire array is approximated as a zero-thickness shell of mass, and the radial equation of motion is solved numerically in the azimuthally symmetric case while also coupling the evolution of the load inductance to the generator circuit. This calculation is less straightforward for a planar array, which lacks cylindrical symmetry and for which load inductance is a more complicated function of geometry than the cylindrical case. A technique for performing a 0D-type simulation for an arbitrary arrangement of wires and return current structures has been developed, however, and was employed by A. A. Esaulov (University of Nevada, Reno) in collaborative design of the planar array loads for the May-June 2007 Saturn shots. Termed the "wire dynamics model" [11], the technique can be applied to single or multiply nested cylindrical arrays, or planar wire arrays. The model implicitly includes inductive division of current between the wires at each time step, and essentially applies Newton's second law to each wire (modeled as a 0D current-carrying filament with some prescribed mass per unit length) in order to track its trajectory. For a cylindrical array, this is equivalent to the standard thin-shell 0D implosion model, but this approach is more general. Inductive current division still allows current to be distributed throughout the wires in a planar array, but causes current to peak in the few wires near the edge of the array with the outermost wires carrying a factor of 2-3 times more current than the innermost wires [11]. We expect this to be the most reasonable assumption for planar arrays, given the observations that the inner wires ablate and so must carry some current [8], but also that the inner wires experience little acceleration while the implosion commences at the outer wires and cascades inward [11, 13] implying that somewhat less current flows in the inner wires. Modeling with inductive division best reproduces the latter observation. We note, however, that modeling of the planned Saturn planar loads was also carried out by A. S. Chuvatin (Ecole Polytechnique) with the assumption of uniform (i.e. resistive) current division between the wires, and similar implosion times, peak currents, and coupled energies were obtained.

The application of 0D-type modeling to planar wire arrays was discussed in detail in
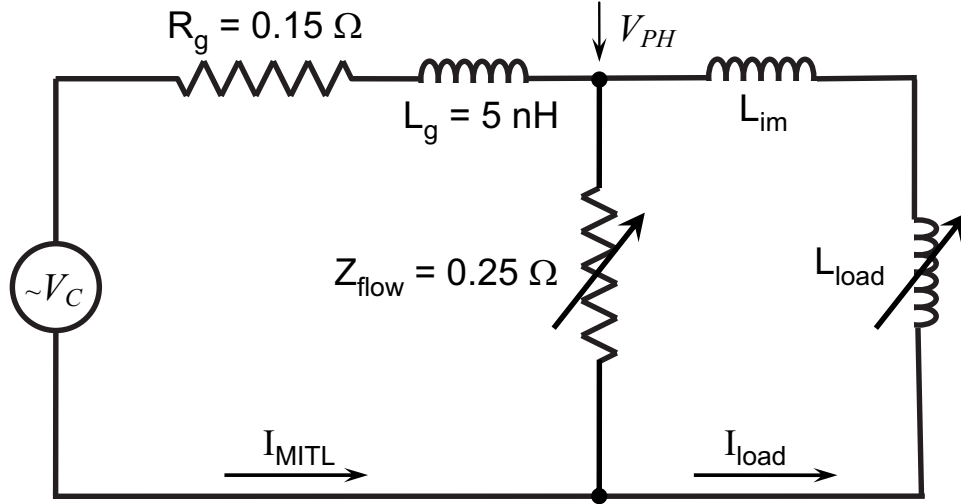
Figure 2.2. The Saturn generator in short pulse mode
was modeled with the equivalent circuit shown in performing
0D-type implosion calculations. Courtesy of C. A. Jennings
(1641) and A. A. Esaulov (University of Nevada, Reno).

Ref. [1]. In Saturn short pulse mode, the equivalent circuit was modified according to
Fig. 2.2, with an open circuit voltage waveform based on analysis of prior short pulse
shots (courtesy of C. A. Jennings) [22]. Generator resistance R_g=0.15 Ω is expected
for Saturn with 36 modules, as was used in August 2008. Generator inductance is
L_g=5 nH. Z_{flow}=0.25 Ω was assumed based on comparison to a limited number of
recent short pulse shots using the 12 inch convolute [19]. As will be shown, how-
ever, higher peak load currents were measured compared to the pre-shot predictions,
which suggests that the 6 inch convolute losses were less than anticipated (or that the
modeled load inductance or L-dot was higher than in the experiment). Inner MITL
inductance L_{im} and load inductance L_{load} were different for planar and compact cylin-
drical arrays. Since the planar array load hardware was identical in 2007-2008, the
calculations of inner MITL and load inductance in Ref. [1] apply to the August 2008
planar array experiments (L_{im} = 5 nH, initial L_{load} = 4.5-7.9 nH for width = 20-8
mm). The same 0D implosion model was used to design 3 mm diameter cylindrical
wire arrays, for which the inductances are calculated analytically from Fig. 2.1 (L_{im}
= 7.9 nH, initial L_{load} = 5.9 nH)). Inductance was quite high for both planar and
cylindrical loads; it would be desirable to field compact loads with a smaller AK gap
on Saturn to increase the load current and to demonstrate coupling to a compact
primary hohlraum.

Pre-shot load design calculations are shown in Table 2.2 for August 2008 planar and
compact arrays. On the one hand, we would like implosion times near 100 ns to be
more directly relevant to the Z current rise. However we do not want the loads to
implode too long after the ∼50 ns current peak in Saturn short pulse mode. Thus,

Table 2.2. Predicted planar and compact cylindrical wire array load behavior, calculated with a 0D-type code including a Saturn circuit model in advance of the experiments and used to guide the choice of load parameters in Table 2.1. The table shows results assuming 100% participation of the initial mass in the implosion; assuming 50% mass participation results in implosion times ∼15 ns shorter. Table 3.1 lists experimental results for comparison. Courtesy of A. A. Esaulov (University of Nevada, Reno).

Shot number	Design implosion time	Implosion time (ns)	Peak load current (MA)	Coupled energy (kJ) ($x_f = 500\mu$m)
3744	Nominal	81	4.3	89
3745	Nominal	82	4.4	88
3746	Nominal	82	4.4	88
3747	Nominal	81	4.3	89
3748	Nominal	85	4.5	76
3752	Nominal	85	4.5	76
3753	Early	59	4.7	103
3754	Earlier	51	4.2	84
3755	Early	59	4.7	103
3756	Earlier	51	4.2	84

we had 60-70 ns implosion times in mind as a design target. In fielding 3 MA planar arrays on Saturn previously [1] and in 3 mm diameter cylindrical arrays on Zebra [9], there was evidence for ∼50% mass participation in the implosion. The model results in Table 2.2 assume 100% mass participation, but the loads were also modeled with 50% mass participation, resulting in estimated implosion times ∼15 ns earlier.

In the case of the 3 mm diameter cylindrical arrays (shots 3753-3756), very large masses were required to reach estimated implosion times >60 ns. This raised concerns regarding the ionization energy required of the generator, and regarding the potential for high opacity of the final radiating z pinch (A. S. Chuvatin, L. I. Rudakov). Thus, we chose shorter implosion times in order to reduce the mass. Still, the heaviest of these loads was equal in mass per unit length to a typical 20 mm diameter tungsten wire array on Z, with a predicted implosion time of only 51 ns at an estimated 4.2 MA. The very high mass and potential opacity of these ultra compact cylindrical arrays may significantly hamper their ability to compete as high-power, compact x-ray sources. Planar arrays have mass with a more significant spatial spread, which provides somewhat lower masses and may be an advantage in avoiding excessive opacity.

In choosing the wire sizes and masses in Table 2.1, the 0D-type code was used itera-

tively for each shot to arrive at a wire size that met the implosion time requirement given the specified array width and wire number. Another constraint was available wire sizes in the Center 1600 inventory, which for a few shots limited the choice of array mass so that an exact match in predicted implosion time was not possible for all shots in the width scan experiment. As will be seen in the section of this report discussing the experimental results, these predictive simulations did a reasonable job of accurately predicting the load current via the Saturn circuit coupling. Although the pre-shot predicted implosion times were somewhat late, the general trends were captured and the initial guess that the loads would exhibit ∼50% mass left behind was supported. This reduced mass participation along with reduced convolute loss and higher measured load currents than predicted resulted in measured implosion times ∼20 ns shorter than the predictions in Table 2.2. Post-shot comparison between the experimental results and the model can be used to refine the circuit parameters for better fidelity in future shot planning. In particular, Z_{flow} can be reduced to obtain better load current agreement.

Table 2.2 also indicates the **jxB**-coupled energy for each shot simulation. This is the kinetic energy of the imploding mass for the single cylindrical wire arrays. For the planar wire arrays, it also includes energy that is dissipated as the wires collide sequentially during the implosion. Momentum is conserved during each collision, but energy is not and the lost kinetic energy is tracked by the code in order to quote the total coupled energy via **jxB** work at the end of the simulation. As with 0D models of cylindrical arrays, an effective final position for the implosion front must be specified at which the simulation will end and the **jxB** work will cease. In these simulations, that final value was taken as $x_f = 500$ μm, based on x-ray imaging that will be presented. We can consider this to be a reasonable estimate of the coupled energy due to **jxB** work. The issue of energy coupling will be discussed further in the context of post-shot simulations of experimental data presented below.

Description of x-ray diagnostics

In May-June 2007, XRDs, PCDs, and bolometers were fielded on both LOS A and LOS B. Fairly close agreement was observed between these two lines of sight, and so in August 2008 XRDs and bolometers were fielded only on LOS B. This LOS viewed the planar wire arrays at an azimuthal position perpendicular to the plane of the wire array, and thus had the best view of the stagnated pinch. LOS views for the planar arrays are shown in Ref. [1] Fig. 2.8, and for the compact cylindrical arrays are shown in Fig. 2.1(b). Radiated power and yield comparisons between 2007-2008 data below all use LOS B data. Two bare Ni bolometers [23] were fielded in 2008, and the measured total x-ray yields (differing by 10-15%) were averaged. A 5 μm kimfol filtered x-ray detector (XRD) [24] was normalized to the average yield in order to quote peak x-ray power. This waveform was integrated in order to quote yield in the pre-pulse (defined as the time prior to the extrapolation of the 20-80% rise to

zero), yield to peak power, and yield in the main x-ray pulse (defined as to the back side of the FWHM). A 2 μm kimfol filtered XRD was also fielded on LOS B, however this was not used in 2007 Saturn shots and so we use the 5 μm kimfol filtered XRD data for consistency. Lambertian correction for an optically thick surface radiator was performed on the bolometer yield (and thus x-ray power) data quoted, but at the 35° viewing angle this amounted to only a -5% adjustment from the calculated 4π (optically thin emission) values. There is a concern for Al loads that the K-shell photons can pass through the 5 μm kimfol filter above 1 keV and dominate the XRD signal over the photons passing through the lower transmission carbon window [25], however this is more of a concern for shots such as on Z where a very significant fraction of the total radiated power ($\sim$30%) is emitted in the Al K-shell range.

Photoconducting detectors (PCDs) [26, 27, 28] filtered with 8 μm Be + 1 μm CH were also fielded on LOS A and B to look at radiated power at photon energies > 1 keV. In the case of the Al z-pinch studied (shot 3748), these can be used quantitatively to determine the K-shell power and yield. For this analysis, it is assumed that all of the K-shell energies is emitted at the Al Ly-α photon energy (1.7 keV) for purposes of performing a filter transmission correction. This is the brightest line observed spectroscopically, and the filter transmissions are high enough at the K-shell energies ($\geq$80 %) that the resulting error due to uncertainty in the spectral shape is less than 10%. Power and yield values quoted represent the average of 4π and Lambertian-corrected values due to uncertainty in the opacity of the K-shell emission, but as noted above this is a small adjustment. We expect Al K-shell power and yield values quoted to be accurate to 25%. For tungsten pinches, whose PCD signals are smaller than for Al K-shell, the detectors are likely responding to the tail of a broad continuum, and so quantitative analysis of PCD data is not practical without detailed and accurate spectral shape characterization data which are not available. It is still useful in some cases, however, to qualitatively observe when the > 1 keV photon emission is turning on for W loads.

A pinhole camera diagnostic was also fielded on LOS B to perform 1 ns gated x-ray imaging of the planar array implosions in order to study their dynamics. As shown in Fig. 2.3, this instrument includes three 8-frame microchannel plate cameras. Two cameras (MLM1 and MLM3) view the z pinch via reflection from multilayer mirrors, which act as monochromators and reflect narrowband photons in the 100-700 eV x-ray range. For these experiments, two Cr/C mirrors were fielded to reflect 277 eV photons with < 10 eV bandpass as shown in Fig. 2.3(b). The third camera (labeled MLM2 but not incorporating a mirror) is a standard filtered pinhole geometry, and 8 μm Be + 1 μm CH was employed to image > 1 keV photons. A similar version of this diagnostic supports x-ray imaging on the Z machine [29, 30, 31, 32]. The Saturn version of instrument is described in Ref. [33].

A time-integrated crystal spectrometer (TIXTL) [34, 26] was fielded on LOS C for one shot only (3748) to measure the Al and Mg K-shell lines. This instrument used a convex KAP crystal with 2 inch bending radius and 20° crystal rotation with a 1/3
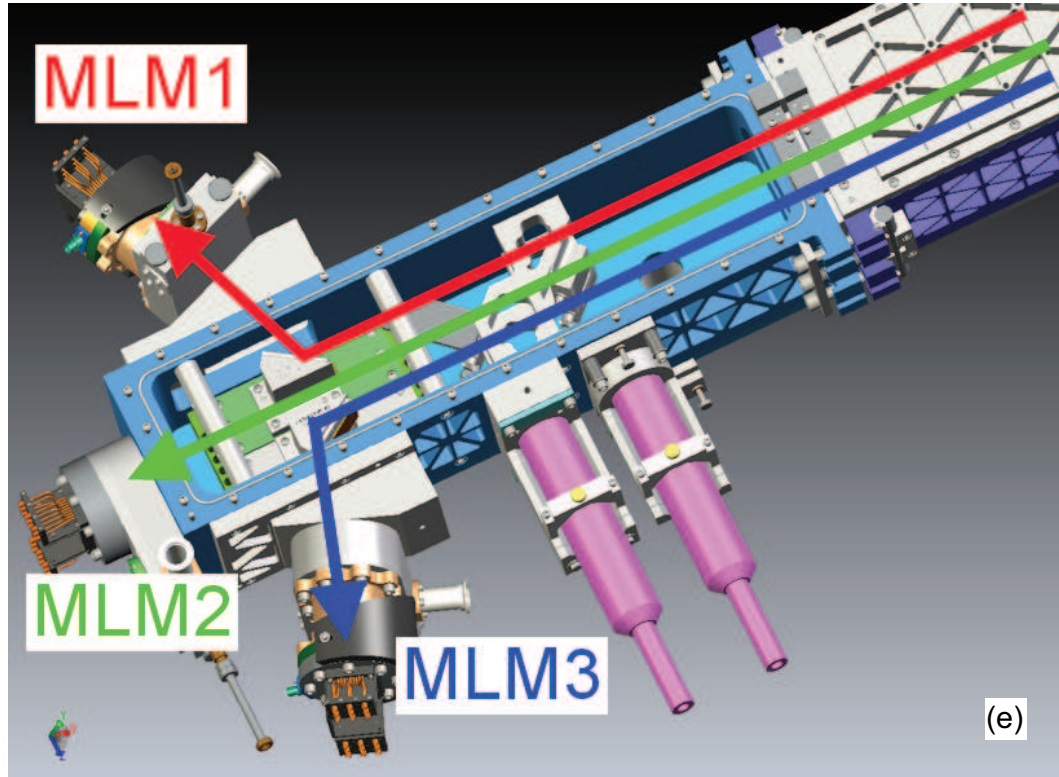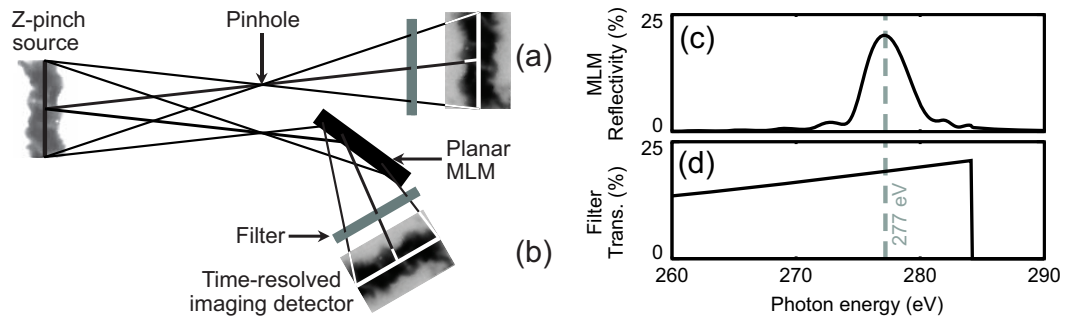
Figure 2.3. A time-resolved pinhole camera diagnostic is employed on Saturn which includes both standard filtered pinhole cameras (a) and pinhole cameras that reflect from a multilayer mirror monochromator (b). The multilayers reflect a narrow band of photons near 277 eV (c) while an aluminized CH filter attenuates visible light and second order reflection (d). The Saturn instrument (e) combines two eight-frame 277 eV photon energy MLM cameras (MLM1, MLM3) with an eight-frame standard pinhole camera (MLM2) filtered for > 1 keV photons. Figures (a-d) are reprinted with permission from B. Jones *et al.*, "Monochromatic X-Ray Self-Emission Imaging of Imploding Wire Array Z-Pinches on the Z Accelerator," IEEE T. Plasma Sci. **34**, 213 (2006), Figs. 1, 2. ©2006, IEEE.

mil Be filter and a 300 μm slit for one-dimensional (axial) spatial resolution of $\sim$900 μm at 1/2 magnification. Al 5056 wires were used for this shot, which have a 5% Mg dopant content so that Mg K-shell lines are less likely to be affected by opacity than Al lines (although it is still a consideration given the relatively high mass fielded).

Electrical diagnostics on these Saturn shots included MITL B-dots and Saturn-type load B-dots for measuring MITL and load current. Load B-dots were fielded in four positions in 2008 (0°, 90°, 180°, 270°) instead of two positions as in 2007 (0°, 180°). The 0° and 180° B-dots shared an identical azimuthal position relative to the rectangular return current can used in the planar array experiments; this was the B-dot position for GI-type sensors fielded in 2007. The 90° and 270° positions were added in 2008 to look for azimuthal asymmetry in the current flow due to the asymmetric load geometry. These B-dot load current measurements were found to agree closely, indicating that any azimuthal asymmetry in the current feed was < 10%, similar to the current measurement error. All four B-dots were averaged in load current measurements indicated below. Resources were not available for fielding an inductive voltage monitor in 2008.

Diagnostic timing errors found in 2007 [1] were corrected, and timing verified by various diagnostic comparisons, over several shot series prior to August 2008. Note that a timing error in the pinhole image timing was identified after the publication of Ref. [1]; images were actually 5.5 ns later in time than reported. Timing is now expected to be accurate to 1 ns on Saturn.

Chapter 3

Discussion of Experimental Results

As discussed above, shots 3744-3747 and 3752 were tungsten planar wire arrays at ~ 5 MA for extending the power scaling study of Ref. [1] to current levels relevant to the multi-pinch vacuum hohlraum concept of Fig. 1.1. Shot 3748 was an Al 5056 planar wire array at $\sim$5 MA to be compared to the $\sim$3 MA planar Al shot 3688 [1] and previous cylindrical Al arrays on Saturn in order to evaluate planar wire arrays as K-shell x-ray sources. Finally, shots 3753-3756 were 3 mm diameter cylindrical tungsten wire arrays in order to provide preliminary data on this configuration as a highly compact x-ray source.

Table 3.1 shows measured load current, implosion time, x-ray rise time and FWHM (LOS B XRD measurements) for all of the August 2008 compact wire array shots. Table 3.2 indicates the measured x-ray yields in the prepulse, rise to peak, main pulse, and total pulse (LOS B data). These tables also indicate the calculated coupled energy estimated with the 0D-type code described above which was in this case run post-shot using measured load current waveforms rather than including the Saturn circuit model. We consider this to be our most reliable estimate of $\mathbf{j}$x$\mathbf{B}$ input energy for each shot. In the following sections we will plot and make reference to these data, but they are included in tabular form here for completeness in this report.

We note that the implosion times listed in Table 3.1 are somewhat shorter than the pre-shot predictions in Table 2.2. As mentioned, this is in part due to the observed load currents being higher than predictions. We also discuss the role of trailing mass in impacting implosion time below.

Tungsten planar wire array total radiated power and yield scaling

The initial study of Ref. [1] suggested peak x-ray power scaling nearly quadratic for planar wire arrays at 1-3 MA, however we also emphasized that a limited data set was being considered. The August 2008 planar wire array shots 3744-3747 and 3752 have now extended this data set to current levels directly relevant to a multi-pinch vacuum hohlraum concept on Z (Fig. 1.1). In addition, we include in the data

Table 3.1. Experimental data for the Saturn shots described in Table 2.1, including load current from B-dot diagnostics and x-ray pulse timing from a 5-μm-kimfol-filtered XRD on LOS B. Implosion time is defined as the time of peak total x-ray power relative to the extrapolation to zero of the linear rise of the load current (45-70% of peak current).

[i]Planar array shots used in the current scaling plots of Fig. 3.1.

Shot number	Peak current (MA)	Implosion time (ns)	10-90% rise time (ns)	FWHM (ns)
3744[i]	5.5	57.9	25.6	19.3
3745[i]	5.4	58.4	19.0	21.9
3746[i]	5.3	51.5	16.1	15.8
3747[i]	4.7	61.5	30.8	22.0
3748	5.5	56.6	27.8	18.2
3752[i]	5.7	56.6	33.4	16.3
3753	5.0	43.6	5.7	12.8
3754	4.4	45.1	6.7	13.6
3755	5.1	53.4	6.5	10.6
3756	4.6	46.1	6.6	11.4

Table 3.2. Experimental total radiated x-ray power and yield data from 5-μm-kimfol filtered XRD normalized to the average of two bare Ni bolometers on LOS B for the Saturn shots described in Table 2.1. Calculated coupled energy is from 0D-type modeling using the measured current waveform and assuming $x_f = 500\mu$m, 100% of the initial mass participating in the implosion (courtesy of A. A. Esaulov, University of Nevada, Reno).

[i]Planar array shots used in the current scaling plots of Fig. 3.1.

Shot number	Peak power (TW)	Yield in prepulse (kJ)	Yield to peak power (kJ)	Peak power ×FWHM (kJ)	Yield to back of FWHM (kJ)	Total yield (kJ)	Calculated coupled energy (kJ)
3744[i]	8.3	16.6	100.2	160.2	162.2	245.3	93
3745[i]	10.5	18.0	140.4	230.4	236.9	298.7	108
3746[i]	15.3	23.0	120.6	242.4	247.0	326.2	108
3747[i]	6.1	14.0	87.8	134.5	143.0	206.8	72
3748	11.5	24.2	138.6	209.3	217.7	287.3	145
3752[i]	13.2	0.5	189.5	215.0	274.6	352.5	135
3753	4.5	0.9	16.8	57.3	46.3	114.6	47
3754	7.2	3.1	30.4	98.2	92.6	155.2	34
3755	4.3	3.5	19.8	45.8	43.4	123.3	48
3756	6.2	3.8	27.2	70.8	61.2	126.8	38

set recent planar array experiments at > 1 MA [35] achieved using a load current multiplier [36]. These shots were 10 mm tall, while the rest of the Saturn and Zebra data were 20 mm tall, however the powers and yields per unit length appear to follow the same trends as will be shown (future Zebra shots will compare 10 mm and 20 mm length loads directly). These Zebra shots 1297 and 1396 are listed in Table 3.3 along with the Zebra shots discussed in Ref. [1]. Radiated power and yields were measured and analyzed in a similar fashion for the Zebra shots as for the Saturn experiments (filtered XRD normalized to bolometer yield, main pulse energy defined as to the back of the FWHM, etc.). As will be discussed, the full final data set is sufficient to allow more reliable analysis of x-ray power and yield scaling, as well as multivariate fitting to include dependence on array width and implosion time.

Table 3.3. Planar wire array experiments on the Zebra generator with approximately matched width, wire number, and implosion time for power scaling comparison with 8- and 12-mm-wide Saturn loads. All arrays used W wire and were 20 mm tall, except 1297 and 1396 which were 10 mm tall. These two arrays both had a 30 μm diameter Al wire placed at one edge of the array for spectroscopic doping and employed a load current multiplier. Courtesy of V. L. Kantsyrev (University of Nevada, Reno).

Shot number	Array width, W (mm)	Wire number	Wire diameter (μm)	Array mass (mg/cm)	Implosion time (ns)	Peak load current (MA)	Peak power (TW)
1249	11.5	24	5	0.091	110	0.80	0.58
1250	11.5	24	5	0.091	110	0.82	0.57
1251	7.5	16	8.9	0.192	105	0.88	0.48
1252	7.5	16	8.9	0.192	125	0.88	0.49
1297	7.7	12	16	0.447	90	1.2	0.54
1396	8.0	17	12.7	0.399	115	1.21	0.4

Shot number	Yield in prepulse (kJ)	Yield to peak power (kJ)	Yield to back of FWHM (kJ)	Total yield (kJ)
1249	0.23	3.3	7.7	11.5
1250	0.65	3.1	7.4	12.9
1251	0.26	1.8	6.7	12.9
1252	0.28	3.6	7.1	13.9
1297	1.1	5.1	8.8	22
1396	0.23	3.6	9.2	11.7
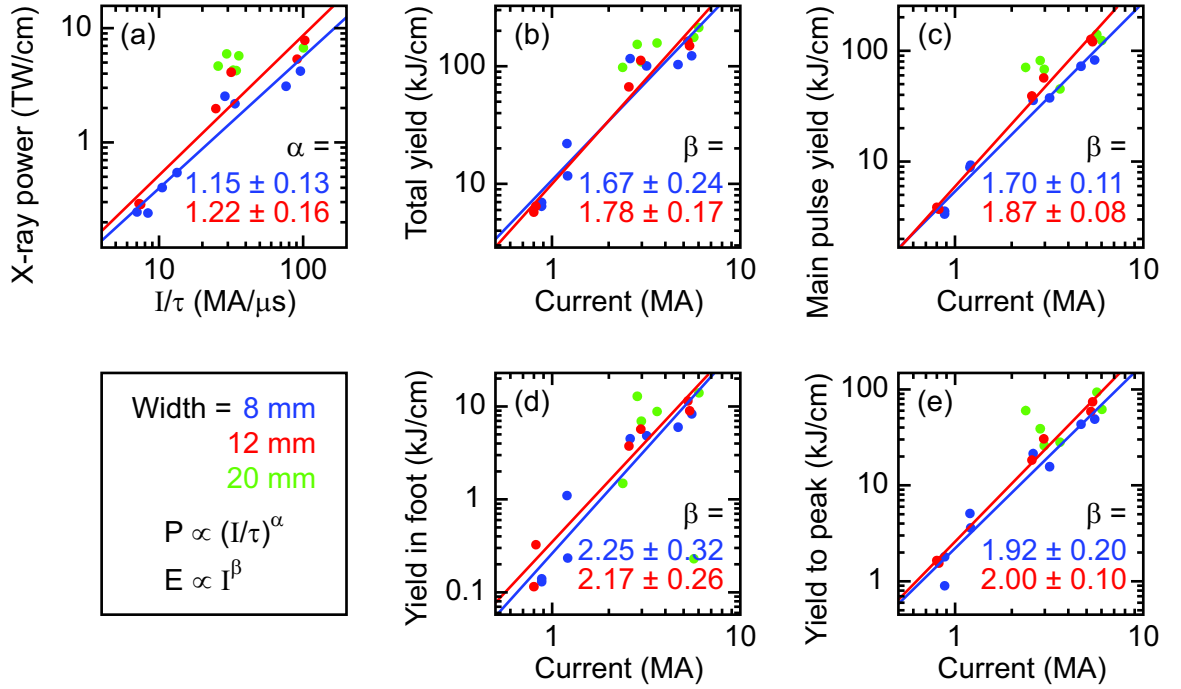
Figure 3.1. Planar array x-ray power and yield scaling with peak load current from Zebra experiments in Table 3.3, Saturn shots indicated in Tables 3.1 and 3.2, and experiments indicated in Ref. [1] Fig. 3.3. The expanded data set now accesses current levels that are directly relevant to multi-pinch configurations on Z. Data exist over a wide enough range of current for 8- and 12-mm-wide loads to allow least-squares fitting to study scaling. Power scaling is seen to be subquadratic with load current divided by implosion time. Yield scaling is closer to quadratic with peak load current. These trends are similar to compact cylindrical wire arrays studied on Z. Zebra data courtesy of V. L. Kantsyrev (University of Nevada, Reno).

Figure 3.1 shows x-ray power and yield scaling plots using Zebra experiments in Table 3.3, Saturn shots indicated in Tables 3.1 and 3.2, and experiments indicated in Ref. [1] Fig. 3.3. The low-current Zebra experiments were constrained by the smallest sizes of available tungsten wire; 20 mm wide arrays were not fielded on Zebra as the required wire size would have been impractical, but 8 mm and 12 mm were possible. Thus, for 8 mm and 12 mm loads we can consider scaling in the current range of 0.8-6 MA. The 20 mm loads were studied over too restricted a range of current to consider current scaling at this array width.

Scaling of peak x-ray power per unit length (P) with load current divided by implosion time (I/τ) is studied in Fig. 3.1(a). The higher current Saturn shots were significantly

shorter implosion times ($\sim$60 ns) than the majority of the shots ($\sim$100 ns), and so some form of current normalization is required. Implosion times also varied for the Zebra shots, which was not accounted for in the initial scaling fits of Ref. [1]. A least-squares fit of the form $P \propto (I/\tau)^{\alpha}$ indicates $\alpha \approx 1.2$ for both 8 mm and 12 mm planar array widths, as shown in Fig. 3.1(a). Sub-quadratic scaling of radiated power with a very similar exponent was noted in Ref. [37] for compact tungsten cylindrical arrays on Z. That work suggests that power from cylindrical arrays may theoretically scale as $(I/\tau)^{3/2}$ in an ablation-dominated regime or else as I^2/τ in a MRT-dominated regime. Repeating the least-squares fit for power per unit length versus I^2/τ gives exponents of 0.66±0.07 and 0.71±0.08 for the 8 mm and 12 mm wide planar loads, respectively, also indicating that the scaling is sub-quadratic.

As x-ray yield is expected to depend on current but not on implosion time [37], we plot total yield, main pulse yield (power curve integrated to back of FWHM), yield to peak x-ray power and pre-pulse yield versus current in Figs. 3.1(b-e). Least-squares fitting to these energies of the form $E \propto I^{\beta}$ give scaling much closer to quadratic. Again, the best-fit exponent on the scaling of total yield is in close agreement with the behavior of compact tungsten cylindrical arrays on Z [37].

Following the completion of the August 2008 planar array shots, the full Saturn and Zebra tungsten planar array data set is substantial enough to allow multivariate fitting in order to determine the power law dependence of x-ray power and yield on load current, implosion time, and array width. These are the key parameters for which scaling must be understood in order to pursue numerical design of a multi-pinch vacuum hohlraum concept on Z. The fitting is performed with a regression analysis tool which has previously been applied to compact tungsten cylindrical arrays on Z [38]. The results of the multivariate fits are shown in Table 3.4. The power law exponents are all fairly well constrained, as the data set includes scans over each of the dependent variables, i.e. a current scan at both 8 mm and 12 mm widths (Fig. 3.1), a mass (implosion time) scan and a width scan at $\tau \sim$100 ns [1]. Though the 20 mm width points (green) in Fig. 3.1 do not cover a wide enough range to determine current scaling of 20 mm arrays in that figure, they do contribute to the width dependence in the multivariate fitting. While plotting power versus I/τ in Fig. 3.1(a) we are constraining the exponents of I and τ to be equal, however these are allowed to be independent in the more general multivariate fit.

It is very interesting that the empirical scaling behavior of planar and cylindrical wire arrays are so similar. This suggests that similar heating mechanisms are important in both wire array geometries. Phenomena such as wire ablation, precursor formation, opacity of the stagnated pinch, and resistive heating may be playing a role in both cases. It is desirable to understand the implosion dynamics and energy coupling mechanisms relevant to planar wire arrays in order to motivate the observed power scaling based on physics principles. This is a difficult task for any z-pinch geometry, and we start to address this in the following section. While we will not be able to fully explain the physical origin of the scaling behavior here, it is worth emphasizing

Table 3.4. Multivariate fitting is performed to all of the tungsten planar wire array shots in Tables 3.2, 3.3, and Ref. [1] Table 3.3 (minus the shots with broken wires and dirty MITLs). Power per unit length (P), and yields per unit length are fit versus power law dependence on peak load current (I), planar array width (W), and implosion time (τ). Multivariate scaling fits to Z compact tungsten cylindrical arrays [38] are shown for comparison; load radius (R) replaces planar array width here.

	Planar wire arrays	Cylindrical arrays (Z)
$P \propto$	$I^{1.28\pm0.13}W^{0.96\pm0.24}\tau^{-0.64\pm0.12}$	$I^{1.45\pm0.10}R^{0.71\pm0.21}\tau^{-1.34\pm0.17}$
$E_{total} \propto$	$I^{1.71\pm0.15}W^{0.45\pm0.27}\tau^{0.30\pm0.13}$	Not available
$E_{main\ pulse} \propto$	$I^{1.68\pm0.12}W^{0.64\pm0.21}\tau^{0.07\pm0.10}$	$I^{1.94\pm0.12}R^{0.58\pm0.25}\tau^{0.33\pm0.20}$
$E_{foot} \propto$	$I^{1.94\pm0.44}W^{-0.32\pm0.78}\tau^{-0.06\pm0.39}$	Not available
$E_{peak} \propto$	$I^{1.78\pm0.16}W^{0.77\pm0.28}\tau^{-0.17\pm0.14}$	Not available

again that the empirical result includes data very near in parameter space to planar array loads that could be fielded on Z as part of a multi-pinch vacuum hohlraum concept as in Fig. 1.1.

The scaling of Table 3.4 can be used in numerical modeling to determine what would be the optimal number of primary hohlraums, width of planar arrays, etc. For example, a configuration with four 12-mm-wide planar arrays driven in parallel by 26 MA and imploding in 110 ns on Z is predicted to output P =5.9±0.2 TW/cm, $E_{main\ pulse}$ = 158±5 kJ/cm, and E_{total} = 308±12 kJ/cm for each 20 mm tall pinch (errors reflect the least-squares fitting; shot-to-shot variation would greater, based on Saturn load behavior). It seems clear that lower total x-ray power would be obtained compared to a double-ended vacuum hohlraum using two 20 mm diameter cylindrical wire arrays, and so the reduction in hohlraum surface area would have to be significant enough to compensate and still produce competitive hohlraum temperatures. Detailed numerical modeling with a 3D viewfactor code (R. A. Vesey) is required to quantitatively assess and optimize the multi-pinch vacuum hohlraum concept.

Further experiments could study higher wire number planar arrays or other variations that might narrow the pulse and produce higher x-ray powers. Also, it is worth noting that a Z experiment would likely use 10 mm tall planar arrays and hohlraums. The Saturn planar loads were all 20 mm tall, necessary to provide a view of an adequately large fraction of the pinch height given the large return current cage structure and 35° LOS view. It is desirable to study variation of x-ray power and yield with pinch height prior to planning a Z configuration. This will be studied later this year on Zebra (V. L. Kantsyrev), and experiments could be considered on Saturn using 10

mm tall planar arrays with a closely coupled return current cage (desirable to reduce inductance and primary hohlraum surface area, as well as to provide an adequate axial view factor).

Planar wire array implosion dynamics

Figure 3.2 shows current and x-ray power/yield data for shot 3746, which we will discuss here as an example of the post-shot analysis using the 0D-type modeling. A linear fit to the 45-70% rise of the measured load current, capturing the linear rise stage of the current waveform, is used to define the time base. The extrapolation of this line to zero current gives the t=0 point for purposes of defining the implosion
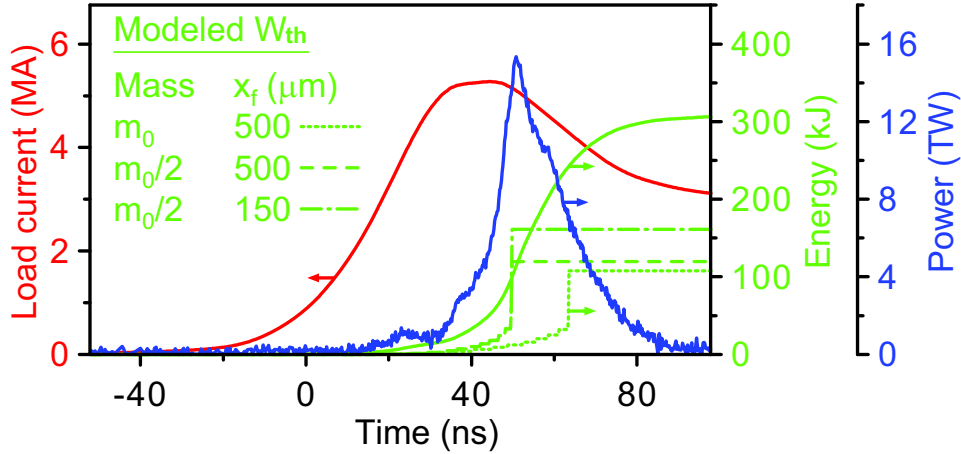
Figure 3.2. Post-shot 0D-type modeling of the experiment using the measured load current waveform for shot 3746. Measured (LOS B) total radiated x-ray power is shown (blue) along with integrated x-ray yield (solid green) and measured load current (red). The time base is relative to the extrapolation of the measured 45-70% linear load current rise to zero. Calculated thermalized energy (W_{th}) is shown for several mass participation and final pinch size conditions (dashed green curves). The calculated implosion time with 100% mass participation is later than the experiment; reducing the implosion front mass by 50% provides better agreement. Calculated **jxB** input energy cannot explain the total measured x-ray yield. Explaining the energy in the main pulse (to back of FWHM) requires very high convergence and small final pinch size. Modeling courtesy of A. A. Esaulov (University of Nevada, Reno).
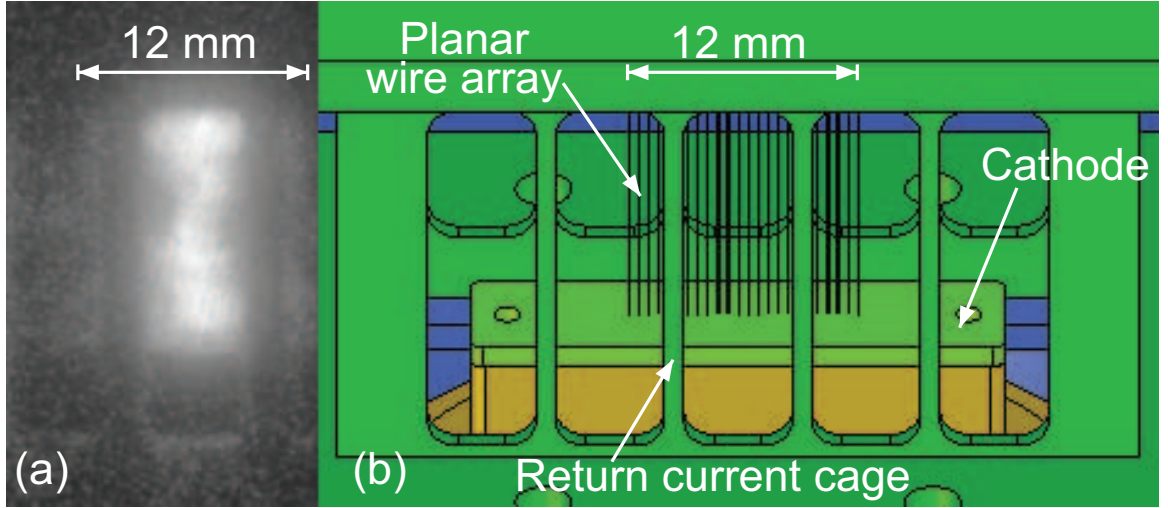
Figure 3.3. (a) A 277 eV self-emission image from 12-mm-wide planar array shot 3746, ∼1-ns-gated at +0.2 ns relative to peak x-ray power shows emission extending to the initial position of the outer wires. The image is displayed with a log gray scale to emphasize the dim emission from the trailing mass, which is likely lower temperature and density than the stagnated plasma on axis. (b) A drawing of the load region as viewed at 35° from the horizontal by the LOS B imager. Courtesy of M. Vigil (1675).

time (the time of peak x-ray power) in Table 3.1. The same procedure was applied to modeled load currents in defining the implosion times in Table 2.2 and in the post-shot simulations.

For all of these 2008 Saturn planar array shots, it is found that even using the measured load current waveform in the simulation, the implosion time is still too late relative to the measured x-ray power pulse. This is apparent for the coupled energy estimate in which the simulation was performed assuming 100% mass participation in the implosion front (dotted green curve). Agreement with the measured time of peak x-rays can be obtained by using only 50% of the initial array mass in the simulation. This can be interpreted as evidence that significant mass (∼50%) trails the leading implosion front due to MRT instability. This same observation was made for 3 MA planar wire arrays on Saturn [1]. Evidence for trailing mass extending to the initial outer wire position of a planar wire array at the time of peak x-ray power is shown in Fig. 3.3.

A similar conclusion has been reached for cylindrical wire arrays at 1-20 MA [39, 40, 41], where it was concluded that 30-50% of the mass may trail behind the fastest implosion front at the foot of the power pulse. The fraction of mass left behind

the implosion may be exacerbated in planar wire arrays, however. Simulations of cylindrical wire arrays using a 3D MHD code indicate that the current prefers a lower inductance path, and so flows in the azimuthal direction in order to shunt out of MRT imploding bubbles [42]. The ability of the current to flow azimuthally has the effect of allowing the MRT to heal itself to a certain extent, as the current tries to stay at larger radius and gather up trailing material. Due to the quasi-2D geometry of planar wire arrays, there is no azimuthal current path possible for current to shunt out of the MRT bubbles, and so the current should continue to drive these all the way to the axis. This could be a detrimental effect, leading to large MRT spatial broadening of the imploding mass, or it could be a positive effect leading to robust gap formation and high convergence in the MRT bubble regions. At the same time, the distributed mass in planar wire arrays is expected to help stabilize MRT growth during the implosion as the implosion front continues to snowplow wire material [11, 12, 13] (analogous to nested cylindrical arrays). It is not clear which of these effects will dominate the performance of planar wire arrays. This would be interesting to study using a resistive 3D MHD code, which could capture the diffusion of the current through MRT spikes and assess whether the trailing material is brought in later by the current or is completely left behind by the implosion.

In Fig. 3.2, the W_{th} curves shown are the integrated energy thermalized at each collision between adjacent wires such the final value is the total **jxB**-coupled energy in the simulation. We note that these values are very similar for the 50% (dashed green curve) and 100% (dotted green curve) mass participation cases, indicating that our 0D-type estimate of the coupled energy is not terribly sensitive to the mass fraction participating in the implosion and stagnation. Comparing these to the x-ray power pulse (blue) and integrated x-ray yield (solid green), we see that the code calculation of coupled **jxB** energy cannot explain the total radiated yield. Explaining even the energy in the main pulse would require high convergence and final pinch radius < 100 μm; calculated coupled energy is shown assuming 150 μm final radius as that is the smallest final size that is consistent with analysis of the inductive voltage monitor from the 3 MA Saturn shot 3685 (E. M. Waisman) [43]. Inability to explain the main pulse x-ray yield based on calculated **jxB**-coupled energy was similarly observed for all 3 MA Saturn planar arrays [1].

These observations suggest that Ohmic heating is playing a significant role in depositing energy in the plasma. It has been noted previously that (due to their distributed and large mass) planar wire arrays are expected to couple less kinetic energy than cylindrical wire arrays, and so resistive effects should be more apparent [8]. For the one Saturn shot (3685) where the inductive voltage probe was successfully fielded, an "energy balance procedure" circuit analysis in the manner of Ref. [43] also indicates the resistive nature of this planar wire array load as shown in Fig. 3.4. The procedure gives a lower bound for the resistance of the pinch, which is seen to peak at > 0.3 Ω on the back side of the main x-ray power peak. The corresponding Joule dissipation dominates the energy deposition in the load at late times.
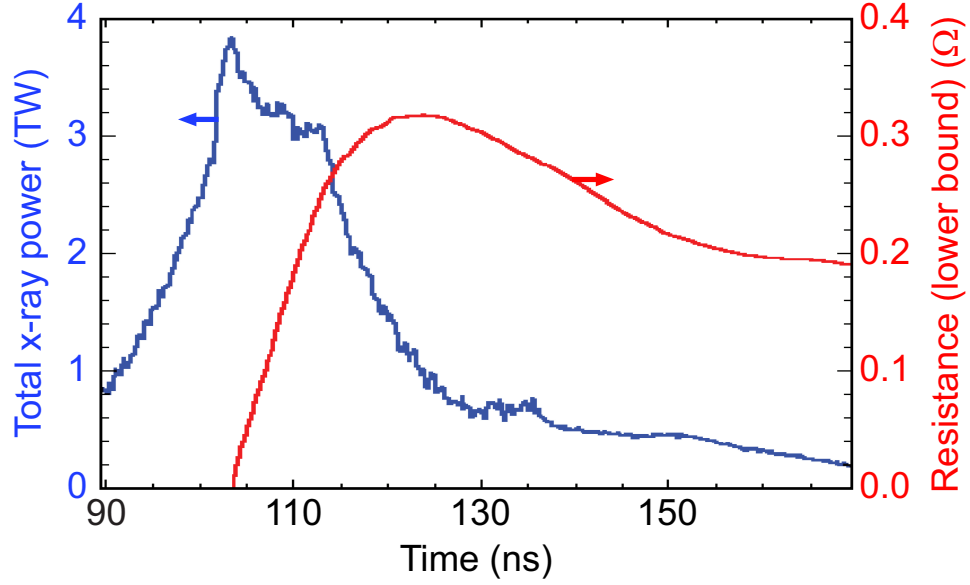
Figure 3.4. The "energy balance procedure" of Ref. [43] is applied to one 3 MA, 100 ns Saturn planar array shot (3685) with an inductive voltage probe fielded. The analysis gives the lower bound for the pinch resistance versus time (red curve). The total radiated power pulse (blue curve) is shown for comparison. Given this large resistance, Ohmic heating dominates the plasma energy deposition in the later part of the stagnation phase. Courtesy of E. M. Waisman.

Resistive heating is likely important during the production of the main x-ray pulse, as evidenced by the inability of the calculated **jxB**-coupled energy to explain this radiated yield. It is also interesting to study the 0D-type model of Fig. 3.2 in greater detail to assess the rate at which the Lorentz force does work on the plasma. The energy thermalized (W_{th}) in the 0D-type planar array implosion model is the integral of a series of delta functions corresponding to energy dissipation when the implosion front collides with each adjacent wire. We expect the implosion front to have some width due to MRT instabilities, and we can represent this phenomenologically by broadening each delta function prior to summing. This was performed for the 0D-type model with 50% mass participation and $x_f = 150$ μm (Fig. 3.2, dash-dotted green curve), with each step broadened into an asymmetric Gaussian with left and right half-widths motivated by the experimental x-ray power pulse. With a smoothly varying W_{th} constructed in this way, the derivative then gives the rate at which the **jxB** force is doing work on the plasma. This is plotted along with the x-ray power in Fig. 3.5. The shapes of the two pulses agree, however the amplitudes are different by a factor of two. To the degree that the W_{th} smoothing function was chosen correctly, this indicates that **jxB** work cannot explain the rate at which the plasma is radiating energy during the main x-ray pulse. However, a narrower smoothing function perhaps
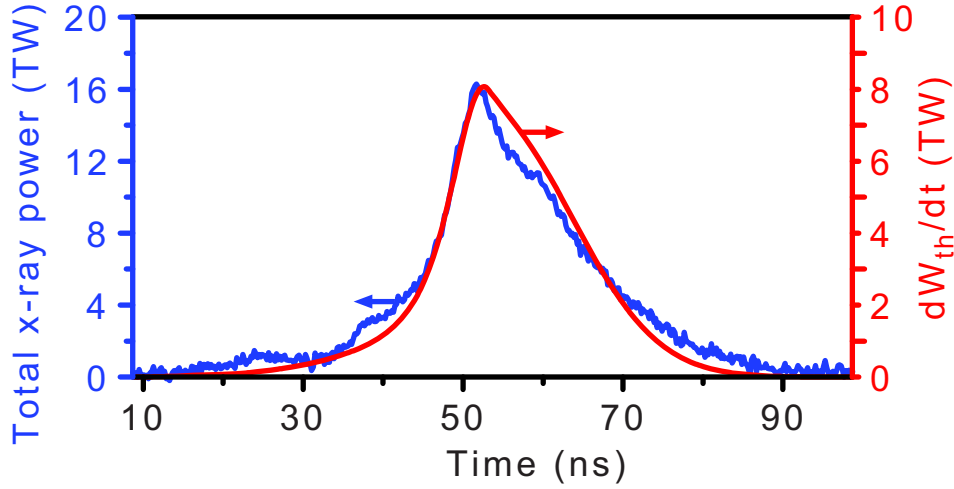
Figure 3.5. The measured total x-ray power pulse shape (blue) from planar array shot 3746 can be matched by an appropriately smoothed thermalized energy (W_{th}) calculated with a 0D-type model. The time derivative dW_{th}/dt (red) gives the rate at which **jxB** work is performed on the plasma. One can construct a matching pulse shape, however the radiative loss rate exceeds the energy deposition rate by a factor of two. This **jxB** energy deposition cannot explain the radiated power, suggesting that Ohmic heating must also be heating the z pinch. Modeling courtesy of A. A. Esaulov (University of Nevada, Reno).

could have increased the deposited power early in time, accounting for the initial rise of the radiated power, but leaving a larger deficit (which must be made up by Ohmic heating) during the later part of the power pulse. It would be appealing to choose the smoothing function based on measurements of the MRT-broadened implosion front width and the implosion velocity, and this analysis may be revisited.

We also employ time-gated pinhole imaging in order to study the planar array implosion dynamics. Soft x-ray self-emission imaging data at 277 eV photon energy from the 12-mm-wide planar array shot 3746 are shown in Fig. 3.6 as the red component of the images. Pinhole imaging data filtered for > 1 keV photons were also obtained at times from -19.2 to +3.4 ns relative to peak x-ray power. These data are the green component of a subset of the images in Fig. 3.6(a), so that yellow indicates the overlay of 277 eV and > 1 keV photons. A clear edge to the implosion front is seen in part (a), although there is axial variation including bright spots emitting both 277 eV and > 1 keV photons at several locations along the edge of the dimmer 277 eV emission filling the interior volume. The bright spots and the edge of the dimmer emission are aligned. The observation that the bright spots emit > 1 keV photons suggests that the temperature at those locations is significantly higher than elsewhere, and the fact
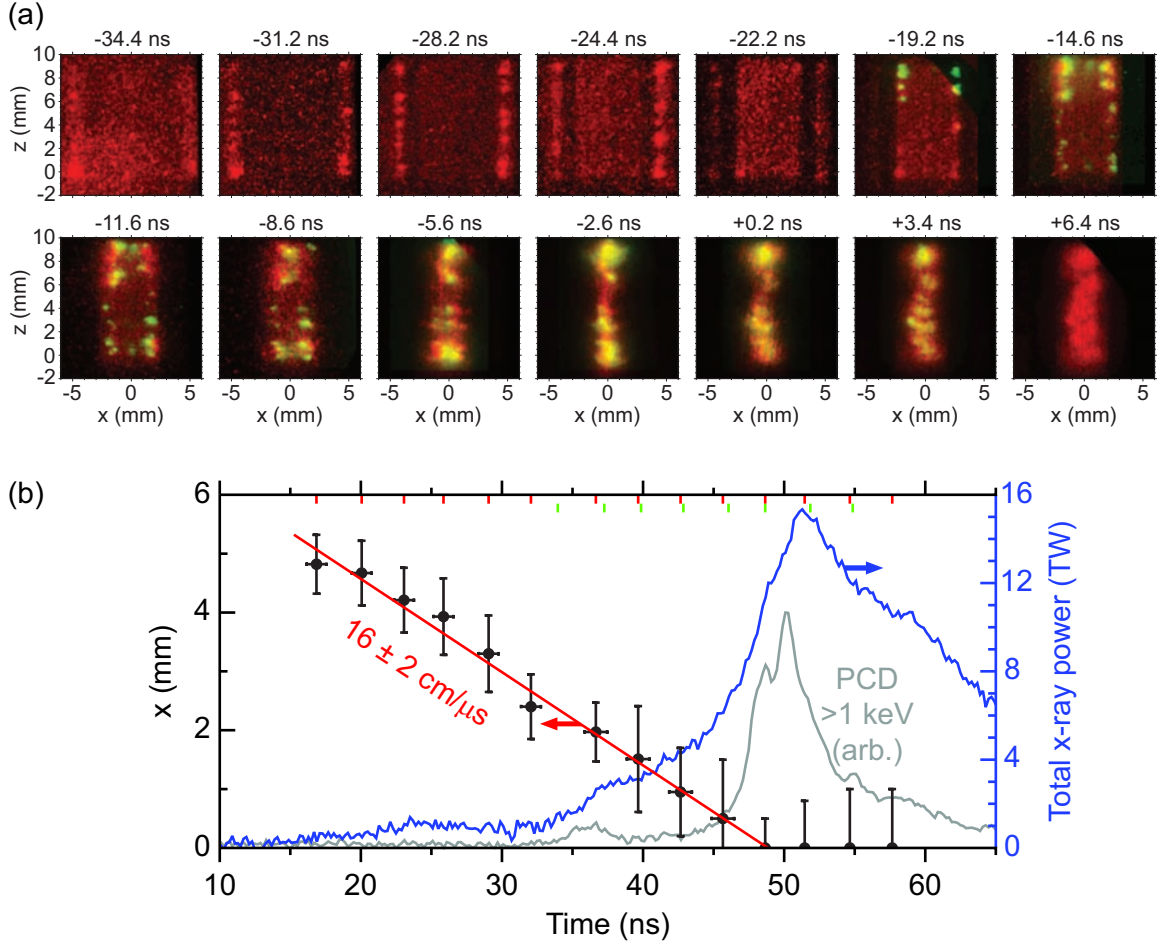
Figure 3.6. (a) Soft x-ray 277 eV self-emission images from shot 3746 (MLM1 frames 3-8, MLM 3 frames 1-8) are shown in red. Pinhole images filtered for > 1 keV (MLM2 frames 1-8) are shown in green (yellow when overlayed with red) for times from -19.2 to +3.4 ns relative to peak x-ray power. (b) Timing of 277 eV and > 1 keV images are shown at the top of the plot by red and green tick marks, respectively. The emission front trajectory inferred from the 277 eV images is shown (black circles) with error bars indicating the fit width of the front. A linear fit (red line) to the first 11 points yields the indicated implosion velocity. Total x-ray power (blue) is shown for comparison, and the > 1 keV PCD signal (gray) is shown in arbitrary units.

that they dominate both 277 eV and > 1 keV images suggests that the density is high. In the following we assume that this emission front represents the leading edge of the imploding mass, i.e. the magnetic-Rayleigh-Taylor-induced bubbles which in cylindrical arrays deliver significant mass and kinetic energy to the axis [44]. These MRT bubble locations would be shock heated during implosion due to snowplow of wire material, and thus should be both hot and dense. Self-emission is generally dependent on both density and temperature, and so resistive 3D MHD simulations would be valuable to verify the relationship (position, width, and velocity) between the observed emission front and the imploding mass. The 277 eV images are averaged axially and processed through Gaussian fitting as described in Ref. [1] in order to track the trajectory of the implosion front. The frame at -22.2 ns must be estimated by eye, as the bars of the return current cage at $x = \pm 3$ mm obscure the emitting region. Figure 3.6(b) shows this trajectory (black circles), with the error bars representing the Gaussian fit width of the implosion front which may be indicative of the distribution of mass in this imploding layer.

The implosion velocity appears to be constant over the time range of the 277 eV imaging data. This may be reasonable, as the implosion front must continue to snowplow wire core material and likely also ablated pre-fill plasma on its way toward the axis. A linear least-squares fit to the trajectory in Fig. 3.6(b) (red line) gives a velocity of 16 ± 2 cm/μs. This value and error bar are also consistent with tracking individual bright spot pairs in the last few frames before they reach the axis. If only 50% of the mass is participating in the implosion, which is likely given the previous discussion, then the estimated kinetic energy is 25 ± 5 kJ. If we assume that all of the initial wire mass is participating in the implosion at the measured velocity, then an upper bound for the coupled kinetic energy is 50 ± 10 kJ. From Table 3.2, we note that the measured pre-pulse yield was 23 kJ, the yield to peak power was 121 kJ, the yield to the back of the FWHM was 247 kJ, and the total yield was 326 kJ. The calculated coupled energy was 99-112 kJ (corresponding to 100% or 50% mass participation). Only 67-79 kJ of this is kinetic energy in the model, with the remainder being internal energy that is thermalized during collisions between wires as the snowplow implosion progresses. In an MHD model, we might expect closer to a 50/50 split between kinetic and internal energy (this would be worth studying in detail with resistive 3D MHD). Also taking into account the 23 kJ lost to radiation in the prepulse, the measured 25-50 kJ kinetic energy of the implosion is consistent with the 0D-type model estimate. This analysis is again supportive of the earlier statement that the energy coupled by **jxB** work is far from explaining the total yield, and can only account for a portion of the yield in the main x-ray pulse. It is likely that resistive heating must make up the balance of the energy deposition in the plasma which is ultimately responsible for generating x-ray radiation. It would also be worth considering PdV compression by the **jxB** force in the final stagnation through MHD simulation; even with velocity constant, the magnetic field may be doing work against the back pressure of the growing plasma internal energy during the final pinch assembly. The pinhole image and energy coupling analysis discussed here is also consistent with the 3 MA, 100 ns shot 3685 discussed in Ref. [1].

One other caveat to note is that any mass trailing the main implosion front (which must be cold and thus barely visible in the self-emission images of Figs. 3.3 and 3.6) may continue to accelerate after the main implosion front collides on axis, as discussed for cylindrical wire arrays in Ref. [16]. Thus, the total coupled kinetic energy may be greater than the peak instantaneous kinetic energy at the start of the main x-ray pulse. Again, it would be interesting to study the implosion of trailing mass in a resistive 3D MHD simulation in order to understand whether current is present in this material. In possible future Z experiments, x-ray radiography [45] could also answer the question of whether trailing mass brings additional kinetic energy following the main implosion front. It would be valuable to first post-process MHD models to design a ZBL backlighter configuration that could radiography the expected trailing mass above the areal density threshold of the diagnostic.

The total x-ray power pulse and a > 1 keV filtered PCD signal (arbitrary units) are both shown in Fig. 3.6(b). The start of the > 1 keV main rise corresponds to the arrival of the implosion front, suggesting that significant on-axis heating is beginning at that time. The duration of the > 1 keV pulse corresponds approximately to the rise of the total x-ray pulse; this time may be dominated by shock heating and thermalization of kinetic energy. Ohmic heating may become significant when the trailing mass brings the current to the axis at a time near peak total x-ray power. This is qualitatively consistent with the analysis of pinch resistance in Fig. 3.4.

The behavior of the planar array in shot 3746 after the peak of the x-ray pulse in Fig. 3.6 is consistent with observations in Ref. [1]. A narrow ∼1 mm FWHM column is seen at the time of peak x-ray power. Within several nanoseconds after the peak, this column has grown to 2-3 mm FWHM, with noticeable axial striations with a few-mm period on both the 277 eV and > 1 keV images. This structure then remains quite static for as long as tens of ns after peak power, during the tail of x-ray emission. This structure is suggestive of a non-ideal plasma in which resistivity may be greater than the Spitzer value in a uniform plasma column. The growth in pinch size after stagnation could be due to MHD instabilities, or due to the continued arrival of material on axis, causing the size of the pinch to grow. This could likely be addressed by studying Al planar arrays with time-resolved (and possibly radially-resolved) K-shell spectroscopy; collisional-radiative modeling of the spectra with the added constraint of measured K-shell power may reveal the amount of mass participating in x-ray emission on axis as a function of time. MHD simulations may also offer insight to the final stagnation dynamics.

It is clear from Fig. 3.6 and the 3 MA planar array data of Ref. [1] that significant axial structure exists at all stages during the plasma stagnation. Although these are self-emission images which may depend on both temperature and density, it is reasonable to conclude that there is likely a density variation along the pinch length as required for Hall resistivity to begin to play a role in Ohmic heating [15, 8]. We cannot presently quantify a density contrast parameter from the experimental data, however, and so any modeling of these experiments will have to treat that as a free

parameter adjusted to fit the x-ray power and yield data. While it will be interesting to see if the experimental trends can be reproduced, this is not entirely satisfactory as curve-fitting to an unmeasurable parameter does not provide strong validation of a proposed physical model. It may be possible in future experiments to measure density variation along the z-axis via spectroscopic means, through analysis of the MLM images coupled with collisional-radiative simulations following the discussion of Ref. [32], or through radiography on Z [45]. In the present study, we conclude that there is evidence for Joule heating of the planar array z pinches, but we do not identify the detailed physical mechanism.

Aluminum K-shell radiation from a planar wire array

One shot (3748) in August 2008 used Al 5056 wires in a planar array configuration in order to provide additional data regarding the suitability of planar array geometries for K-shell production. This adds to the ∼3 MA, 100 ns, Al 5056 shot 3688 from the 2007 long pulse Saturn planar array experiments. As discussed previously, it is not obvious that planar arrays should work well for this application, as K-shell excitation typically requires large initial cylindrical array diameters, high velocities, and high coupled energy per ion to achieve high plasma temperatures. The mass distributed internal to a planar array near the axis seems to work against this goal. However, if the planar array geometry leads to higher convergence or enhances resistive heating, then the net result could be positive for K-shell x-ray generation.

Figure 3.7 shows the LOS A and LOS B K-shell power measured by PCDs, along with total x-ray power for pulse shape comparison. The PCD signals peak ∼5 ns earlier than the XRD, and we believe that the data acquisition relative timing is correct. The PCD signals were more noticeably early with the tungsten planar array loads [Fig. 3.6(b)] and may indicate higher temperatures during the rise of the total x-ray power. We use the LOS B K-shell measurements in the following, as LOS A has a restricted field of view of the stagnated pinch (less axial height is viewed, and return current cage may aperture the emission in the horizontal direction). The total Al K-shell yield was about 17 kJ at a load current of 5.5 MA (Table 3.1). Table 3.5 summarizes the results of the two Al 5056 planar array loads that have been fielded on Saturn (3688, 3748) as well as the cylindrical wire array from short-pulse Saturn with the highest published Al K-shell yield at 83 kJ [20]. More typical Al K-shell yields on Saturn are ≥ 60 kJ.

At first glance, the planar arrays do not appear competitive with cylindrical wire arrays. However, we note that lower peak current was obtained from planar array shot 3748 in short pulse mode than for cylindrical arrays. One goal for future planar array K-shell studies would be to vary implosion time and reduce initial inductance in order to increase the load current.
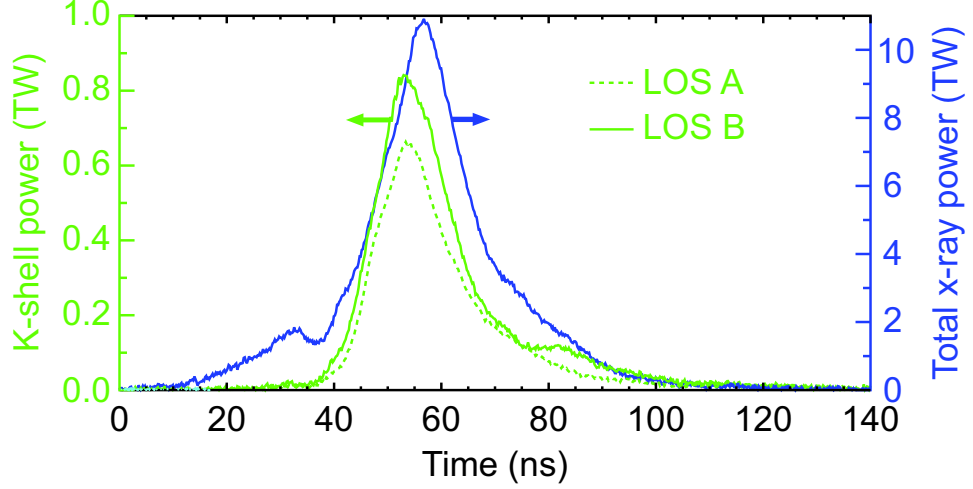
Figure 3.7. Al K-shell power measured with 8 μm Be + 1 μm CH filtered PCDs from Saturn shot 3748. LOS B (solid green) views greater axial pinch height, while LOS A (dashed green curve) may be more significantly apertured by the return current cage. Total x-ray power from a 5 μm kimfol filtered XRD normalized to average bolometer yield (LOS B) is shown for comparison. Total K-shell yield 13.3 kJ (LOS A), 17.2 kJ (LOS B) was a small fraction of the total radiated yield 287 kJ (LOS B).

A second important factor is that the planar arrays were relatively high mass and low η compared to the cylindrical wire array cited. The efficiency parameter η is equal to the energy coupled per ion divided by the minimum energy needed to ionize to the K shell and given by

$$\eta = E_i/E_{min} \tag{3.1}$$

where $E_i = Am_pE_{\mathbf{jxB}}/ml$ is the energy coupled per ion of atomic mass A in a z pinch of mass per unit length m and length l, $E_{\mathbf{jxB}}$ is the total energy coupled by the generator to the load, m_p is the proton mass, and $E_{min} \approx 1.012Z^{3.662}$ eV/ion is the minimum energy to ionize to the K-shell [46, 47, 48]. A general guideline is that $\eta > 2$ is desired in order to generate appreciable K-shell radiation from a z pinch plasma of any atomic number Z. The **jxB**-coupled energy is estimated according to 0D-type modeling in Table 3.6, using measured load current waveforms, and assuming 100% mass participation and $x_f = 500$ μm for the planar arrays listed. As noted earlier, the estimated couple energy does not depend strongly on the fraction of mass participating (Fig. 3.2). η is then calculated from Eq. 3.1 for the cases of 50% and 100% mass participation in Table 3.6.

Table 3.5. Al K-shell x-ray generation results from planar wire arrays on Saturn, compared to the best published Saturn cylindrical wire array result. Typical cylindrical array Al K-shell yields on Saturn are closer to 60 kJ. Calculated η is shown, obtained with 0D-type implosion modeling. The range in η for planar arrays corresponds to assuming 100% or 50% mass participation in the implosion.

Shot	Load	Current (MA)	τ (ns)	K-shell yield (kJ)	K-shell main pulse (kJ)	K-shell power (TW)	η
3688	20 mm planar	3.6	90	11	6	0.36	1.6-2.8
3748	20 mm planar	5.5	60	17	12	0.84	2.1-4.6
14*	30 mm cylindrical	7.5	75	83	58	2.4	8.5

*Shot results quoted from Ref. [20].

Table 3.6. K-shell scaling model of Ref. [48] applied to the Al wire array shots of Table 3.5. Cases of 50% and 100% participation of the initial mass m_0 in the implosion are considered for the planar wire arrays. The calculated **jxB**-coupled energy and η are indicated. For planar arrays, 0D-type calculations use the measured load current waveform and assume $x_f = 500$ μm. For shot 14, $E_{\mathbf{jxB}}$ is calculated from the η value in Ref. [20]. K-shell model parameters are calculated using $c\,(Z = 13)$=47, scaled from the Ar value in Ref. [48].

Shot	m_0 (mg/cm)	100% mass participation $E_{\mathbf{jxB}}$ (kJ)	η	f	S	Y_K (kJ)	50% mass participation $E_{\mathbf{jxB}}$ (kJ)	η	f	S	Y_K (kJ)
3688	0.47	64	1.6	0.04	1	2.4	57	2.8	0.18	1	10
3748	0.79	145	2.1	0.04	1	5.2	157	4.6	0.23	1	36
14	0.41	301	8.5	0.3	0.91	82	NA	NA	NA	NA	NA

42

We can attempt to be more quantitative in assessing the K-shell x-ray performance of the loads by applying the K-shell yield scaling model of Ref. [48]. In this work, a phenomenological model for K-shell yield is formulated and benchmarked to single cylindrical wire array data from the Z machine. The model is further discussed and benchmarked to nested cylindrical Z arrays in Ref. [49]. To briefly summarize the model, the estimated K-shell yield is given by

$$Y_K = fSE_{\mathbf{jxB}} \tag{3.2}$$

The scaling parameter S is less than unity at relatively low mass and low current and the pinch is said to be in an inefficient regime (Y_K much less than total yield) with K-shell yield small but scaling rapidly as $Y_K \propto I^4$. When $S = 1$, the radiation source is said to be efficient with as much as 30% of the total radiation emitted from the K shell, and yield scaling as $Y_K \propto I^2$. The term f can be as high as 0.3 in this model, but is less when the effect of radiative cooling at high mass and low η removes energy from the plasma before it can contribute to exciting K-shell emission. In this case, $f \propto c\,(Z, \text{load})\,\eta^{3/2}/m$. These K-shell yield model parameters are calculated in Table 3.6 for the two Al planar array loads and one cylindrical array example. The scaling coefficient is taken as $c\,(Z = 13, \text{load}) = 47$, scaled as $Z^{2.9}$ from the value benchmarked to Ar implosions per Ref. [48]. This coefficient can depend on the configuration of the load, and we might expect it to be different for planar arrays compared to cylindrical arrays due to the differences in implosion dynamics discussed earlier. Nevertheless, we will apply the scaling model to the Al planar shots under study and see what can be learned.

We note first of all that the scaling model of Ref. [48] does a reasonable job of approximating the measured K-shell yield from cylindrical Al wire arrays on Saturn (compare Tables 3.5 and 3.6). This load is seen to be low enough mass that the impact of radiative cooling is unimportant ($f = 0.3$, its maximum allowed value), and the load is right at the transition point between inefficient and efficient radiation regimes ($S = 0.91$). In contrast, the scaling model calculations for the planar wire arrays indicate that these high mass, low η loads are likely significantly impacted by radiative cooling ($f < 0.3$). The scaling model predicts K-shell yields that are too low if we assume 100% mass participation; we could re-benchmark the Y_K model and increase $c\,(Z, \text{load})$ if we wanted to continue to use a 0D-type implosion model assuming 100% mass participation. However, we argued earlier that $\sim$50% of the mass could be left behind in the implosion, and with this assumption the scaling model shows factor-of-two agreement with the measured K-shell yields. We have taken 50% mass participation to be representative here, but for a more complete comparison we should iterate on the 0D-type model calculation to choose a mass participation fraction that provides the best agreement with implosion time for each shot (since the modeled Y_K is senstitive to the mass fraction). The coefficient $c\,(Z, \text{load})$ may also need to be re-benchmarked to the measured data in this case.

From this analysis, it seems clear that the Saturn Al planar wire arrays studied to

date had masses that were too great and η that was too low for effective K-shell x-ray production. The effects of radiative cooling in sapping energy from the system so that it could not drive K-shell photon production may be significant. Mitigating this phenomenon would require significantly larger width planar arrays so that mass could be reduced and η increased while maintaining implosion times appropriate for the generator. As mentioned, the inductance of such a load and the attainable peak current also must be considered. Saturn short pulse mode (and shorter implosion time in general) is favored to meet the goals of low mass, high η, and high current. Reaching the same η in long pulse mode would require larger initial array width.

This situation exhibits essentially the same concerns that drive mid-Z cylindrical wire array K-shell x-ray sources to large diameters on the Z machine [50, 49]. As discussed in Ref. [49], the approach to designing a large-width Al planar array on Saturn would be to choose a consistent 0D-type model formulation for estimating $E_{\mathbf{jxB}}$ (i.e. fixed x_f or convergence ratio, fixed mass participation fraction), use this to benchmark $c\,(Z, \text{load})$ to the measured planar array K-shell yields in Table 3.5, and then use the same 0D-type implosion model and Y_K scaling model with this coefficient to design new loads.

We have neglected in the above a discussion of how resistive heating in the pinch would impact the K-shell x-ray production. The presence of Ohmic heating would enhance the coupled energy to the load, which should be beneficial to K-shell production. This is implicitly neglected in our use of a 0D-type model to estimate $\mathbf{jxB}$-coupled energy with the assumption that this is the only energy driving K-shell emission (often assumed for cylindrical K-shell x-ray sources as well). Since we do not have a validated physical model for the scaling of the pinch resistance, we are unable to do better at this time. Ohmic heating is likely also present in cylindrical wire arrays, but it may have much less relative impact in large diameter, high velocity implosions where kinetic heating probably dominates. The impact of Ohmic heating may end up being folded in to the $c\,(Z, \text{load})$ coefficient in the fitting procedure described above. One would have to design and execute additional planar array shots to determine if this modeling approach holds over a wider range of mass and η. Fundamentally, though, K-shell x-ray generation should follow the same basic principles in any load. The question is whether a simple design model can capture the coupled energy in a manner that scales appropriately with load parameters. Consideration of mass and η should be the same in any load, with $c\,(Z, \text{load})$ empirically capturing the hydrodynamic differences in the implosion character of each load. The intuition that it may be difficult for planar arrays to achieve high η and compete with cylindrical loads may turn out to be correct, but could be assessed further.

Another potential problem with planar wire arrays as K-shell sources that is worth noting is that their non-cylindrical geometry could exacerbate azimuthal variations in radiated power and yield. In particular, significant trailing mass could create much higher opacity in off-normal viewing directions. The absence of trailing mass in the direction perpendicular to the plane of the wires could help to mitigate opacity for

these sources, which could benefit the K-shell output, however azimuthal variation of the emission is undesirable for applications of the source and one might be limited by the requirement for K-shell power and yield measurements 180° opposite in azimuth from any test object in order to characterize the source at that azimuthal position. The geometry of the return current cage itself may limit the access to the source compared to a cylindrical load (requiring Be posts and introducing other complications).

The LOS C time-integrated crystal spectrometer (TIXTL) was fielded on shots 3688 and 3748, and spectra were obtained showing the typical Al and Mg K-shell lines (e.g. Ly-α, He-α, Li-like satellites). The Al Ly-α line was observed to be of greater intensity than the Al He-α line, which implies high electron temperature likely in the $T_e > 500$ eV range, although detailed analysis is needed in order to be conclusive. Non-LTE kinetic modeling in the manner of Ref. [51] is presently being carried out by A. S. Safronova (University of Nevada, Reno) to interpret these data and infer plasma conditions in the stagnated plasma. This analysis may confirm that suitable temperatures were obtained for ionization to the K-shell, and the Saturn short and long pulse experiments can be compared along with Zebra Al planar wire array data. It will also be valuable to infer the ion density and (with pinhole images showing the pinch diameter) estimate the mass participation fraction in the K-shell emission. It would also be interesting to compare the measured density with that obtained in a typical cylindrical array Al 5056 implosion; this might provide evidence of whether greater convergence ratios might be achieved in planar wire arrays as suggested previously. Higher convergence due to lack of azimuthal current paths in the mass left behind could be the best hope for K-shell production in planar wire arrays. This would provide higher $E_{\mathbf{jxB}}$, but also leaving mass behind would provide higher η, less radiative cooling, and significantly better K-shell production as indicated in Table 3.6.

Initial study of highly compact cylindrical wire arrays at multi-MA currents

As discussed in the introduction, highly compact soft x-ray source configurations are required in order to drive a secondary vacuum hohlraum with multiple radiation sources as depicted in Fig. 1.1(a). In the previous sections, we made a thorough study of planar wire arrays as a primary candidate for this multi-pinch vacuum hohlraum concept. We are not limited to planar wire arrays, however, and can consider any potentially high-power compact x-ray source geometry. Below, we consider highly compact cylindrical wire arrays of 3 mm initial diameter. In experiments at 1 MA on Zebra, compact cylindrical wire arrays of diameter < 8 mm were found to produce higher x-ray powers and yields than larger, lower mass arrays [8]. High x-ray output was retained down to an array diameter of 3 mm [9], and thus we chose this diameter for initial studies on Saturn. We note that the Zebra optimization may only hold

at 1 MA (where larger arrays also had very low wire number), and larger diameters could be optimal at higher currents. Arrays of 4-8 mm diameter could be studied in future Saturn experiments, however we thought it would be most interesting to push to the extreme for initial compact cylindrical experiments. Two masses were chosen, the highest (12.0 mg) to provide the best match to the Saturn short pulse current rise and maximize current per 0D design calculations, and the lowest (6.75 mg) to mitigate potential opacity and ionization energy concerns (L. I. Rudakov, A. S. Chuvatin). The load parameters are shown in Tables 2.1 and 2.2.

The load current, x-ray power and yield, and other data from the experiments are shown in Tables 3.1 and 3.2. These 3 mm diameter loads radiated a maximum of approximately 7 TW in the main pulse and 150 kJ total yield. As for the planar wire arrays, the x-ray power was inferred by normalizing a 5-μm-kimfol-filtered XRD to the average bare Ni bolometer yield (LOS B). We note what could be a significant caveat here, namely that the bolometers exhibited a long tail, significantly longer than that seen on the XRD. This could indicate that a significant number of photons were emitted at low XUV energies not seen by the filtered XRD, and thus the quoted peak x-ray power may be inaccurate. The bolometer signals were too noisy to be differentiated; in the future it may be possible to reduce the dominant bit noise significantly by employing a scope that can handle the DC offset of the bolometer voltage signals (M. C. Jones). There was also a 2-μm-kimfol-filtered XRD available for these shots and those data could be further analyzed, normalizing the signals to the bolometer yields to determine how the inferred power is impacted. A sub-apertured, unfiltered Si diode has also been suggested to respond to softer photons (V. L. Kantsyrev), but unfortunately was not fielded on these experiments. The maximum load current obtained was 5 MA, which slightly exceed the pre-shot prediction in Table 2.2. As mentioned previously, this load was limited to a current lower than is typical of Saturn short pulse wire array experiments due to its high initial inductance; the diameter was small but a relatively large return current canister was used in order to leave room for 4-mm-wide slots for diagnostic access to the entire initial load diameter.

We can make an initial assessment of x-ray power and yield scaling for 3 mm diameter cylindrical wire arrays by comparing the 2008 Saturn shots with 1 MA experiments. Ideally matched scaling experiments (i.e. same wire number and implosion time) are not available, but three reasonably similar 3 mm diameter tungsten wire arrays from the Zebra generator are identified in Table 3.7. Yield is measured with a bare Ni bolometer, and power with a 5-6 μm kimfol filtered XRD normalized to bolometer yield. We follow the same methodology as for planar arrays, plotting peak power versus I/τ and yields versus peak load current, then performing least-squares fitting for power law scaling coefficients. The analysis is shown in Fig. 3.8. The data set is much more limited than for planar wire arrays, so we must consider this an initial assessment of the scaling. It seems fairly clear from Fig. 3.8, though, that the scaling of both power and yield are sub-quadratic, scaling significantly more slowly with current than planar and larger cylindrical wire arrays (Table 3.4). This could be due to opacity limiting the x-ray output of these very heavy (6.75 and 12.0 mg) loads.

Table 3.7. Compact cylindrical W wire array experiments on the Zebra generator (3 mm diameter, 20 mm tall). Courtesy of V. V. Ivanov and V. L. Kantsyrev (UNR).

Shot number	Wire number	Wire diameter (μm)	Array mass (mg/cm)	Implosion time (ns)	Peak load current (MA)	Peak power (TW)
1258	24	5.0	0.091	70	0.84	1.06
1416	16	5.0	0.061	73	0.84	0.71
1418	16	7.6	0.141	87	0.88	0.72

Shot number	Yield in prepulse (kJ)	Yield to peak power (kJ)	Yield to back of FWHM (kJ)	Total yield (kJ)
1258	0.2	5.9	12.14	17.3
1416	0.6	4.2	10.7	14.5
1418	0.8	6.5	10.9	16.1

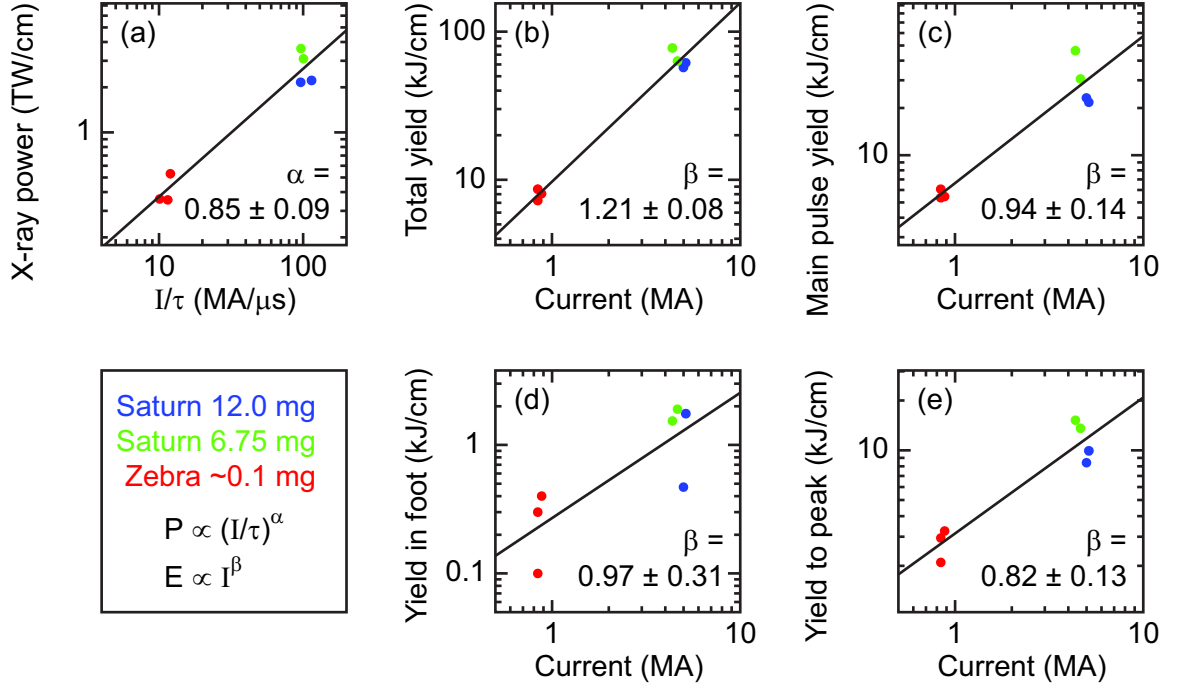**Figure 3.8.** Ø3 mm cylindrical wire array x-ray power and yield scaling from Zebra experiments in Table 3.7, and Saturn shots indicated in Tables 3.1 and 3.2. Power scaling versus I/τ and yield scaling versus I are even further from quadratic than planar arrays or larger cylindrical arrays (Table 3.4). Zebra data courtesy of V. V. Ivanov and V. L. Kantsyrev (UNR).

In Fig. 3.8 the 6.75 mg loads exhibited higher radiated power and yield than the 12.0 mg loads despite the higher load currents of the heavier loads, which supports the notion that high mass may be detrimental. In addition to opacity becoming significant, higher masses require an increasing investment of energy delivered from the generator in ionization of the plasma. These two issues are being considered theoretically (A. S. Chuvatin, L. I. Rudakov) and will be the topic of future work.

In order to discuss dynamics of these compact array implosions, we take shot 3756 as an example. Figure 3.9 shows the measured load current (red), x-ray power (blue), and integrated power (solid green curve). Also shown are 0D-calculated coupled energies assuming 100% mass participation. The calculations are performed for three values of the final radius r_f. Based on > 1 keV pinhole imaging to be shown, $r_f = 300$ μm may be the most reasonable assumed final pinch size. As per the discussion
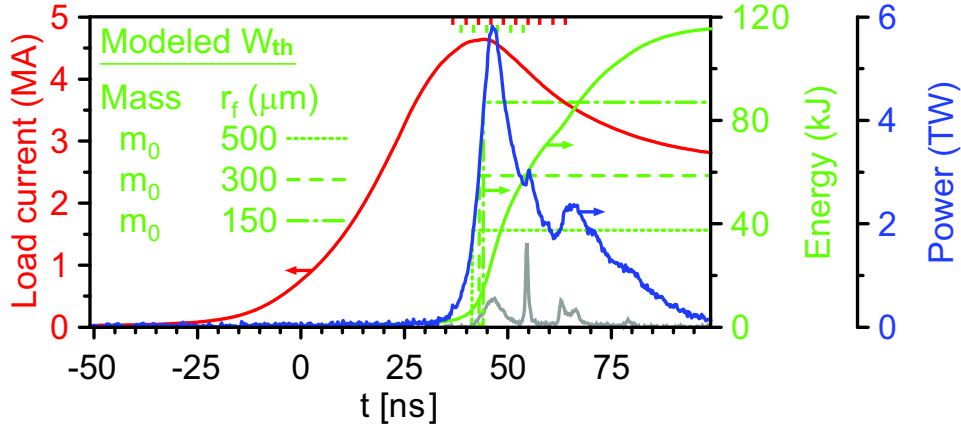
Figure 3.9. Post-shot 0D modeling of the experiment using the measured load current waveform for shot 3746. Measured (LOS B) total radiated x-ray power is shown (blue) along with integrated x-ray yield (solid green) and measured load current (red). A > 1 keV PCD signal is shown in arbitrary units (gray). The time base is relative to the extrapolation of the measured 45-70% linear load current rise to zero. Calculated thermalized energy (W_{th}) is shown for several final pinch sizes (dashed green curves). The calculated implosion time with 100% mass participation is consistent with the time of peak x-ray power, however pinhole imaging clearly shows trailing mass and the implosion is not 0D. Calculated **jxB** input energy cannot explain the total measured x-ray yield. Explaining the energy in the main pulse (to back of FWHM) may be explained with final radius motivated by pinhole imaging. Modeling courtesy of A. A. Esaulov (University of Nevada, Reno).

48

of planar wire arrays, the total radiated yield cannot be explained by the 0D **jxB**-coupled energy unless r_f is taken as unreasonably small. This again implies that resistive heating is important in the z-pinch plasma. Unlike the planar arrays studied, it may be possible to explain the energy in the main x-ray pulse (to back of FWHM) based on the 0D coupled energy.

Per Fig. 3.9, it appears that with 100% mass participation the calculated implosion time agrees well with the time of peak x-ray power. This differs from the planar wire array calculations, in which reduced ∼50% mass participation was required to match the implosion time. From 277 eV time-gated pinhole imaging shown in Fig. 3.10, emission is seen extending to the initial radial position of the wire array. This implies that significant mass is left behind in the implosion, which is also seen in 3 mm
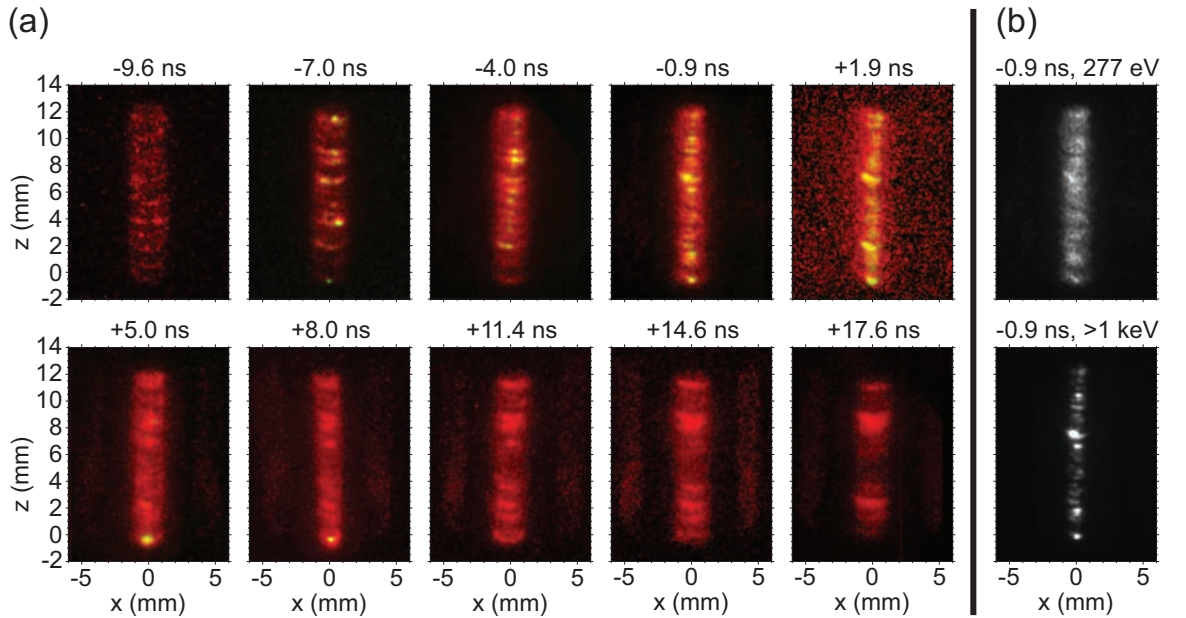
Figure 3.10. (a) Soft x-ray 277 eV self-emission images from shot 3756 (MLM1 frames 6-8, MLM 3 frames 2-8) are shown in red. Pinhole images filtered for > 1 keV (MLM2 frames 3-8) are shown in green (yellow when overlayed with red) for times from -7.0 to +8.0 ns. Frames earlier than -7.0 ns relative to peak x-ray power show no observable > 1 keV emission. Frame timing of 277 eV (red) and > 1 keV (green) images are also shown by tick marks at the top of Fig. 3.9. (b) The 277 eV and > 1 keV images in linear grayscale for the frame nearest the time of peak power. Lineouts across the > 1 keV image indicate ∼0.7 mm FWHM of the emitting column, with individual bright spots having FWHM as narrow as 0.4 mm.

49

diameter arrays at 1 MA through laser shadowgraphy [9]. 3D structure is significant in these implosions, and wire ablation may play a significant role in pre-filling the small array volume. It is certain that the 0D model does not accurately capture the dynamics of these wire arrays in adequate detail.

We can make a few other comments about the implosion dynamics of highly compact wire arrays based on the pinhole imaging data of Fig. 3.10. Laser shadowgraphy in 1 MA experiments on Zebra shows a pronounced $m=0$ structure during the implosion of 3 mm diameter arrays [9]. This may be due to the high global magnetic field, so that from an early time tension in the magnetic field lines works to correlate the implosion instabilities in the wire array. This $m=0$ structure appears to be apparent in the images of Fig. 3.10(a), and so the higher current 5 MA Saturn shots likely share the same implosion dynamics as at 1 MA. It may be that the onset of strong azimuthal correlation is what causes the x-ray power and yield to drop for 1 MA arrays with diameters less than 3 mm per the discussion of Ref. [42]. The axial striations in the images appear as arcs, suggesting that we are viewing (at 35° from the horizontal) only one side of an opaque plasma column with $m=0$ structure. Figure 3.10(b) shows the 277 eV and > 1 keV images obtained from nearest to peak x-ray power on separate linear gray scale plots. The brightest emitting spots in the > 1 keV image are saturated in order to make the emitting column more viewable. From this, it is apparent that the cooler mass radiating at 277 eV extends to 2-3 mm in diameter, while the > 1 keV emission comes from a much tighter column. Taking lineouts across this image, the typical FWHM is $\sim$600 μm. Interpreting this > 1 keV self-emission as being due to a hot, shock-heated central column formed as imploding MRT bubbles arrive on axis motivates choosing $r_f = 300$ μm in the earlier 0D simulations. The series of bright regions seen along the > 1 keV image in Fig. 3.10(b) may correspond to $m=0$ necking regions in the pinch. Also seen are a handful of very intense bright spots with $\sim$400 μm FWHM.

We also note that the last frame of > 1 keV imaging (+8.0 ns) shows a very bright $\sim$400 μm FWHM emitting spot at the cathode ($z=0$) that is a few orders of magnitude more intense than the emission at this photon energy from the rest of the plasma. This corresponds in time to the spike in > 1 keV emission (gray curve) after the main peak shown in Fig. 3.9. Shot 3754 shows this same feature, with an accompanying spike in total x-ray power up to 12 TW. This may be a micropinch caused by an electrode effect [52, 53], but it is curiously small and bright in these shots. From two shots, it is not clear how reproducible this behavior is.

From this initial look at highly compact cylindrical wire arrays, it seems that they are not as strong a candidate for compact soft x-ray sources as planar wire arrays. This could be due to high mass and opacity, in which case investigating 3 mm diameter arrays with a lower Z material could be interesting. If Al were used, then it is likely that the plasma conditions could be studied spectroscopically. It is also possible that the diameter chosen was too small, and perhaps performance could be improved with a 4-8 mm diameter cylindrical wire array (trade-off with hohlraum surface area).

Chapter 4

Conclusion and Future Directions

A series of ten shot were performed with compact wire arrays on Saturn in August 2008. Six of these complement 2007 planar array studies on Saturn. X-ray power and yield scaling to higher current is studied with tugsten arrays, and Al K-shell scaling is also studied at higher current. Four shots fielded 3 mm diameter cylindrical wire arrays to collect initial data to assess their x-ray power and yield scaling to higher current.

A vacuum hohlraum concept was presented in which multiple z pinches are driven in parallel by the pulsed power generator (total current is split among the loads). Each load resides in a magnetically isolated return current structure that also serves as a primary hohlraum. These sources surround a secondary vacuum hohlraum which could be used to produce a Planckian radiation source, or to drive an ICF capsule. To make this concept viable, advanced compact wire array loads are required.

The present Saturn-Zebra planar wire array data set is now complete enough to allow an x-ray power and yield scaling study including current levels directly relevant to a multi-pinch concept on Z. A maximum power of 15 TW (250 kJ in the main pulse, 330 kJ total yield) was obtained at 5.3 MA on Saturn. The full 2007-2008 planar array data set allow multivariate fitting to determine power and yield dependence on load current, implosion time, and array width. The resulting dependence on load current is sub-quadratic for power scaling, and nearer to quadratic for yields. The power law scaling is very similar to results obtained for cylindrical wire arrays on the Z machine previously. With an empirical scaling law in hand for planar wire arrays, the next step is to revisit viewfactor calculations (R. A. Vesey) for various multi-pinch vacuum hohlraum geometries in order to determine through this numerical design assessment if the concept is attractive on the Z machine. As part of this study, a circuit model could be used to assess whether the parallel load architecture can significantly enhance the total current delivered from the generator by reducing the effective load inductance.

A few additional experiments are also required to motivate work on Z. The multi-pinch vacuum hohlraum on Z would use 1 cm tall pinches. In order to allow adequate field of view of the load on Saturn with large AK gaps, all planar array experiments were 2 cm tall. It would be worth fielding 1 cm tall planar wire arrays on Saturn in short pulse mode to verify that the current scaling fit holds when the pinch height is

changed. This experiment would also require significant reduction of the AK gap so that a reasonable fraction of the pinch height could be viewed. Reduction of the AK gaps is also a desired experiment, though, to make sure the load performs well with reduced gaps and to try to increase load current by reducing the initial inductance. Experiments in which planar array height is varied are presently being planned for the 1 MA Zebra facility (V. L. Kantsyrev) which will be a valuable first step in addressing this issue.

Additional Saturn experiments with higher wire number and smaller interwire gaps could help to better stabilize MRT by providing a greater number of hydrodynamic collisions on the way to the axis. Perhaps higher wire number planar arrays would produce narrower pulses and higher x-ray powers more attractive for driving a hohlraum. It could also be worth studying double planar wire arrays on Saturn, in which two parallel linear arrays of wires are placed in close proximity [54]. Work on Zebra indicate they may scale more favorably than single planar arrays [35]. Saturn short pulse experiments at 5-6 MA could establish the scaling of x-ray power and yield up to current levels relevant for a multi-pinch vacuum hohlraum on Z using this alternate load geometry. Double planar arrays also may be better suited to fulfilling ICF pulse shaping requirements than single planar arrays [54].

Estimation of coupled energy through 0D-type implosion modeling and measurement of implosion velocity from pinhole images indicates that **jxB** work cannot explain the yield in the main x-ray pulse for 2007-2008 planar array loads. This suggests that Ohmic heating plays a significant role in energy deposition in these plasmas. This is supported by analysis of one shot fielding a voltage probe in which load resistance $>$ 0.3 Ω was inferred just after peak x-ray power. While resistive heating is desirable for compact x-ray sources (which cannot accumulate significant kinetic energy), it also poses a challenge for physics understanding. A physical model for this resistance is needed in order to motivate scaling to higher load currents. Efforts are ongoing, including assessment of a Hall resistance model (A. S. Chuvatin, L. I. Rudakov).

Analysis of 2007-2008 planar wire array experiments suggests that $\sim$50% of the initial mass may be left behind in the implosion. Post-shot 0D-type implosion calculations using the measured load current require that only 50% of the mass participate in order to match the measured implosion time. Also, 277 eV emission can be seen extending to the initial outer wire position at the time of peak x-ray power. Trailing mass due to MRT growth is typically detrimental to x-ray power production, as it can broaden the imploding mass profile. With their spatially distributed mass, planar wire arrays should better stabilize MRT through snowplow during the implosion. However, MRT growth may also be exacerbated due to the lack of an azimuthal current path, which may force current to flow in the MRT bubbles and drive them to the axis. It is not clear which of these mechanisms are dominant, and for this reason planar wire arrays are an interesting object to study from a z-pinch physics perspective. Resistive 3D MHD simulations would be helpful in order to understand the role of the trailing mass and whether magnetic field can diffuse through it, removing the

driving current. Such simulations could also address the role of Ohmic heating at stagnation, implosion dynamics and partitioning of kinetic and internal energy, PdV work driven by the Lorentz force at the onset of stagnation, impacts of wire ablation and snowplow of mass on the implosion trajectory and velocity, the correspondence between self-emission images and the evolution of plasma density and temperature profiles, and the suitability of radiography for quantifying the trailing mass.

It is possible that the lack of azimuthal current shunting may lead to higher convergence of the MRT bubbles than in cylindrical wire arrays. However, it is also possible that robust gaps will not form and current may reconnect later in the current rise through mass left behind at large radius. It could be interesting to try to make gap formation robust through employing seeded instabilities at the edge wires of the planar wire array. These could be etched wires with modulation of radius [55] or helical wires [56, 57] which have shown better recent success in creating large, discrete gaps. An experiment with seeded perturbations at high current and wire number would be significantly easier to field in a planar array geometry as only the two edge wires would need the perturbation, as opposed to a cylindrical wire array in which all of the wires must have the perturbation properly aligned. An even simpler way to explore this concept would be in a fan-shaped planar wire array in which the wires are more closely spaced at the cathode than at the anode (the 2D analog of a conical array). Like a conical wire array [58] or radial array [59], one would expect the implosion to start at the cathode where the magnetic field is higher. Multiple implosions initiating at this cathode contact point due to current restrike are often observed in radial wire arrays. In the planar geometry, the gaps that must remain clear are reduced to two azimuthal positions.

Two Al 5056 planar wire arrays have been studied to date at Saturn. A preliminary analysis suggests that the K-shell yield may be adequately captured by application of the scaling model of Ref. [48]. This model indicates that for a planar array to produce yields at a level competitive with cylindrical wire arrays, the load mass must be reduced and width increased in order to enhance the efficiency parameter η. This is an identical concern as with mid-atomic-number cylindrical wire arrays on Z. It is possible that the distributed mass of the planar array geometry might better stabilize MRT, however locating so much mass nearer the axis also poses a significant penalty in η. Additional 0D-type modeling could be carried out in order to assess whether a wide Al planar array load looks promising for Saturn short pulse mode. Analysis of K-shell spectra obtained in Saturn Al planar experiments is also continuing (A. S. Safronova), and may provide information about the temperatures and densities achieved in these loads.

An initial assessment of highly compact 3 mm diameter tungsten cylindrical wire arrays indicates power and yield scaling with current that is much further below quadratic than planar arrays or larger cylindrical arrays. This could be due to the very high masses (6.75-12.0 mg) required to match the implosion time to the rise time of the generator even in short pulse mode on Saturn. Theoretical consideration of

opacities and the ionization energy sink for these massive loads are continuing (A. S. Chuvatin, L. I. Rudakov). It could be interesting to try 3 mm diameter arrays on Saturn with a lower-Z material such as Al, Ti, or Cu to study the role of opacity in limiting x-ray power.

The 3 mm loads exhibit $m=0$ structure during the implosion in a manner consistent with 1 MA Zebra studies at this diameter. Increased azimuthal correlation as load diameter is reduced could be the cause of x-ray power degradation. It would be desirable to field slightly larger loads in the 4-6 mm diameter range on Saturn to determine if these emit higher x-ray powers, and to study the structure in the imploding plasma. For 3 mm loads on Saturn, 277-eV-emitting material is seen extending to near the initial radius at and after the time of peak x-ray power. In an experiment with a closely coupled primary hohlraum (return current can), one would likely aperture the pinch significantly in the horizontal direction which would make it difficult or impossible to diagnose the emitted power and yield. Thus, one may be required to study the scaling of these loads in a high inductance geometry which will limit the current.

Additional shots on Saturn could help motivate future Z shots. The highest priority would be to assess 1 cm tall tungsten loads with small AK gaps in support of application of the scaling fits to Z configuration design. This could be done in both short and long pulse mode to bound the Z implosion time. Higher wire number loads could study MRT snowplow stabilization, and double planar wire arrays could be studied. Aluminum planar array shots at larger width could also be beneficial not only to assess K-shell yields, but also to spectroscopically diagnose plasma parameters and address stagnation physics. Valuable for cylindrical arrays as well, time-resolved spectroscopy would provide the maximum insight through addressing the accumulation of mass and heating on axis. Additional shot opportunities with tungsten as well as Al planar arrays would be helpful for understanding dynamics via x-ray pinhole imaging and voltage monitor measurements, and the x-ray radiography and inductance unfold techniques established on the Z machine could be used to further enhance understanding of pinch energetics should shots on that facility be possible in the future. Even a few shots on Z would provide definitive power scaling data to help motivate hohlraum/ICF concept studies using one or more planar wire arrays at high current, as well as radiography data to address the issue of mass left behind. Moderate Z compact arrays could be studied on Saturn to mitigate opacity at high mass. Planar and compact cylindrical arrays pose z-pinch physics questions about trailing mass, opacity, MRT stabilization, and current convergence that merit study with resistive MHD simulation and will likely provide insight relevant to all z-pinch loads.

References

[1] B. Jones, M. E. Cuneo, D. J. Ampleford, et al. Sandia Report No. SAND2007-6337. Office of Scientific and Technical Information (OSTI) of the U.S. Department of Energy (www.osti.gov) Document No. 920806.

[2] C. Deeney, M. R. Douglas, R. B. Spielman, et al. *Phys. Rev. Lett.*, 81:4883, 1998.

[3] R. B. Spielman, C. Deeney, G. A. Chandler, et al. *Phys. Plasmas*, 5:2105, 1998.

[4] M. K. Matzen, M. A. Sweeney, R. G. Adams, et al. *Phys. Plasmas*, 12:055503, 2005.

[5] J. H. Hammer, M. Tabak, S. C. Wilks, et al. *Phys. Plasmas*, 6:2129, 1999.

[6] M. E. Cuneo, D. B. Sinars, E. M. Waisman, et al. *Phys. Plasmas*, 13:056318, 2006.

[7] R. A. Vesey, M. C. Herrmann, R. W. Lemke, et al. *Phys. Plasmas*, 14:056302, 2007.

[8] V. L. Kantsyrev, L. I. Rudakov, A. S. Safronova, et al. *High Energy Dens. Phys.*, 3:136, 2007.

[9] V. V. Ivanov, V. I. Sotnikov, J. M. Kindel, et al. Plasma dynamics and x-ray generation in small-diameter cylindrical wire-array z-pinches. *Phys. Plasmas*, to be submitted, 2008.

[10] B. S. Bauer, V. L. Kantsyrev, F. Winterberg, et al. *AIP Conf. Proc.*, 409:153, 1997.

[11] A. A. Esaulov, A. L. Velikovich, V. L. Kantsyrev, et al. *Phys. Plasmas*, 13:120701, 2006.

[12] A. A. Esaulov, V. L. Kantsyrev, A. S. Safronova, et al. *Phys. Plasmas*, 15:052703, 2008.

[13] V. V. Ivanov, V. I. Sotnikov, A. Haboub, et al. *Phys. Plasmas*, 14:032703, 2007.

[14] M. E. Cuneo, D. B. Sinars, D. E. Bliss, et al. *Phys. Rev. Lett.*, 94:225003, 2005.

[15] A. S. Chuvatin, L. I. Rudakov, and A. L. Velikovich. *AIP Conf. Proc.*, 808:343, 2006.

[16] J. P. Chittenden, S. V. Lebedev, C. A. Jennings, et al. *Plasma Phys. Control. Fusion*, 46:B457, 2004.

[17] A. V. Shishlov, S. A. Chaikovsky, A. V. Fedunin, et al. Microsecond planar wire array implosions on the GIT-12 generator, Oral presentation 4A7. *34th IEEE International Conference on Plasma Science (ICOPS)*, 2007.

[18] B. Jones, C. Deeney, C. A. Coverdale, et al. *J. Quant. Spectrosc. Radiat. Transfer*, 99:341, 2006.

[19] B. P. Peyton and C. A. Jennings. Private communications, 2008.

[20] C. Deeney, T. J. Nash, R. B. Spielman, et al. *Phys. Plasmas*, 5:2431, 1998.

[21] K. W. Struve, T. H. Martin, R. B. Spielman, et al. Circuit-code modeling of the PBFA Z for z-pinch experiments. In *Digest of Technical Papers, 11th IEEE Int. Pulsed Power Conf., Baltimore, MD*, page 162. IEEE, 1997.

[22] C. A. Jennings. Private communication, 2008.

[23] R. B. Spielman, C. Deeney, D. L. Fehl, et al. *Rev. Sci. Instrum.*, 70:651, 1999.

[24] G. A. Chandler, C. Deeney, M. Cuneo, et al. *Rev. Sci. Instrum.*, 70:561, 1999.

[25] Y. Maron. Private communication, 2007.

[26] T. J. Nash, M. S. Derzon, G. A. Chandler, et al. *Rev. Sci. Instrum.*, 72:1167, 2001.

[27] R. B. Spielman. *Rev. Sci. Instrum.*, 66:867, 1995.

[28] R. B. Spielman, L. E. Ruggles, R. E. Pepping, et al. *Rev. Sci. Instrum.*, 68:782, 1997.

[29] B. Jones, C. Deeney, A. Pirela, et al. *Rev. Sci. Instrum.*, 75:4029, 2004.

[30] B. Jones, C. Deeney, C. A. Coverdale, et al. *IEEE T. Plasma Sci.*, 34:213, 2006.

[31] B. Jones, C. Deeney, C. A. Coverdale, et al. *Rev. Sci. Instrum.*, 77:10E316, 2006.

[32] B. Jones, C. Deeney, C. J. Meyer, et al. *AIP Conf. Proc.*, 926:229, 2007.

[33] B. Jones, C. A. Coverdale, D. S. Nielsen, et al. *Rev. Sci. Instrum.*, 79:to be published, 2008.

[34] T. Nash, M. Derzon, R. Leeper, et al. *Rev. Sci. Instrum.*, 70:302, 1999.

[35] K. Williamson. Scaling of radiation parameters of planar and compact cylindrical wire arrays on the 1MA Zebra generator. 7th International Conference on Dense Z-Pinches, 2008.

[36] A. S. Chuvatin, L. I. Rudakov, B. V. Weber, et al. *Rev. Sci. Instrum.*, 76:063501, 2005.

[37] W. A. Stygar, M. E. Cuneo, R. A. Vesey, et al. *Phys. Rev. E*, 72:026404, 2005.

[38] M. E. Cuneo. Results of compact single and nested wire array experiments: scaling and pulse shaping. 6th Wire Array Workshop, 2006.

[39] S. V. Lebedev, F. N. Beg, S. N. Bland, et al. *Phys. Plasmas*, 8:3734, 2001.

[40] S. V. Lebedev, D. J. Ampleford, S. N. Bland, et al. *Plasma Phys. Control. Fusion*, 47:A91, 2005.

[41] M. E. Cuneo, E. M. Waisman, S. V. Lebedev, et al. *Phys. Rev. E*, 71:046406, 2005.

[42] E. P. Yu, M. E. Cuneo, M. P. Desjarlais, et al. *Phys. Plasmas*, 15:056301, 2008.

[43] E. M. Waisman, M. E. Cuneo, R. W. Lemke, et al. *Phys. Plasmas*, 15:042702, 2008.

[44] V. V. Ivanov, V. I Sotnikov, G. S. Sarkisov, et al. *Phys. Rev. Lett.*, 97:125001, 2006.

[45] D. B. Sinars, M. E. Cuneo, E. P. Yu, et al. *Phys. Rev. Lett.*, 93:145002, 2004.

[46] K. G. Whitney, J. W. Thornhill, J. P. Apruzese, and J. Davis. *J. Appl. Phys.*, 67:1725, 1990.

[47] J. W. Thornhill, K. G. Whitney, J. Davis, and J. P. Apruzese. *J. Appl. Phys.*, 80:710, 1996.

[48] J. W. Thornhill, A. L. Velikovich, R. W. Clark, et al. *IEEE T. Plasma Sci.*, 34:2377, 2006.

[49] B. Jones, C. A. Coverdale, C. Deeney, et al. Implosion dynamics and K-shell x-ray generation in large diameter stainless steel wire array z pinches with various nesting configurations. *Phys. Plasmas*, submitted for publication, 2008.

[50] C. A. Coverdale, C. Deeney, B. Jones, et al. *IEEE T. Plasma Sci.*, 35:582, 2007.

[51] A. Safronova, V. Kantsyrev, A. Esaulov, et al. *AIP Conf. Proc.*, 808:149, 2006.

[52] C. A. Jennings, J. Chittenden, T. Sanford, and A. Ciardi. *Bull. Am. Phys. Soc.*, 51:127, 2006.

[53] D. J. Ampleford, C. A. Jennings, M. E. Cuneo, et al. *Bull. Am. Phys. Soc.*, 51:64, 2006.

[54] V. L. Kantsyrev, L. I. Rudakov, A. S. Safronova, et al. *Phys. Plasmas*, 15:030704, 2008.

[55] B. Jones, C. Deeney, J. L. McKenney, et al. *Phys. Rev. Lett.*, 95:225001, 2005.

[56] G. N. Hall, J. P. Chittenden, S. N. Bland, et al. *Phys. Rev. Lett.*, 100:065003, 2008.

[57] G. N. Hall. Modifying wire-array z-pinch ablation structure and implosion dynamics using coiled arrays. 7th International Conference on Dense Z-Pinches, 2008.

[58] D. J. Ampleford, S. V. Lebedev, S. N. Bland, et al. *Phys. Plasmas*, 14:102704, 2007.

[59] S. V. Lebedev, A. Ciardi, D. J. Ampleford, et al. *Plasma Phys. Control. Fusion*, 47:B465, 2005.

DISTRIBUTION:

1 A.A. Esaulov
Nevada Terawatt Facility/372
University of Nevada, Reno
Reno, NV 89557

1 V.L. Kantsyrev
Physics Department/220
University of Nevada, Reno
Reno, NV 89557

1 A.S. Safronova
Physics Department/220
University of Nevada, Reno
Reno, NV 89557

1 V.V. Ivanov
Physics Department/220
University of Nevada, Reno
Reno, NV 89557

1 J. Kindel
Physics Department/220
University of Nevada, Reno
Reno, NV 89557

1 R.C. Mancini
Physics Department/220
University of Nevada, Reno
Reno, NV 89557

1 A.S. Chuvatin
Laboratoire de Physique et Technologie des Plasmas
Laboratoire du Centre National de la Recherche Scientifique
Ecole Polytechnique
91128 Palaiseau
France

1 L.I. Rudakov
Icarus Research
P.O. Box 30780
Bethesda, MD 20824-0780

1 J.W. Thornhill
Naval Research Laboratory
Plasma Physics Division
Radiation Hydrodynamics Branch
Code 6720
Washington, DC 20375

1   C. Deeney
      Director, Office of Defense Science
      NA-11/Forrestal Building
      U.S. Department of Energy
      1000 Independence Ave., S.W.
      Washington, DC 20585

5	MS 1193	B. Jones, 1673
5	MS 1193	M.E. Cuneo, 1673
1	MS 1106	D.J. Ampleford, 1673
1	MS 1159	C.A. Coverdale, 5935
1	MS 1194	E.M. Waisman, 1673
1	MS 1186	R.A. Vesey, 1674
1	MS 1196	D.S. Nielsen, 1675
1	MS 1193	L.B. Nielsen-Weber, 1675
1	MS 1193	R.E. Hawn, 1675
1	MS 1179	J.D. Serrano, 1344
1	MS 1196	J.A. Torres, 1675
1	MS 1193	M.C. Jones, 1675
1	MS 1192	D.A. Graham, 1676
1	MS 1192	S.P. Toledo, 1676
1	MS 1106	R.K. Michaud, 1342
1	MS 1106	D.M. Abbate, 1342
1	MS 1193	M.D. Kernaghan, 1672
1	MS 1193	M. Vigil, 1675
1	MS 1168	D.H. Romero, 1646
1	MS 1186	M.F. Johnson, 1675
1	MS 1186	J.E. Garrity, 1675
1	MS 1193	M.R. Lopez, 1675
1	MS 1192	T.C. Wagoner, 1676

1	MS 1192	R.L. Mourning, 1676
1	MS 1194	J.K. Moore, 1676
1	MS 1194	W.E. Fowler, 1671
1	MS 1106	K.A. Mikkelson, 1342
1	MS 1106	B.P. Peyton, 1342
1	MS 1106	T.A. Meluso, 1342
1	MS 1106	B.M. Henderson, 1342
1	MS 1106	M.A. Torres, 1342
1	MS 1106	J.W. Gergel, Jr., 1342
1	MS 1190	M.K. Matzen, 1600
1	MS 1191	J.L. Porter, 1670
1	MS 1181	T.A. Mehlhorn, 1640
1	MS 1181	L.X. Schneider, 1650
1	MS 1178	D.D. Bloomquist, 1630
1	MS 1168	D.H. McDaniel, 1650
1	MS 1186	M.P. Desjarlais, 1640
1	MS 0125	J.P. VanDevender, 12101
1	MS 1179	M.A. Hedemann, 1340
1	MS 1159	J.W. Bryson, 1344
1	MS 1196	W.A. Stygar, 1671
1	MS 1193	B.W. Atherton, 1672
1	MS 1186	M. Herrmann, 1674
1	MS 1191	G.T. Leifeste, 1675
1	MS 1196	R.J. Leeper, 1677
1	MS 1193	B.V. Oliver, 1645
1	MS 1168	C.A. Hall, 1646
1	MS 1152	M.L. Kiefer, 1652

1	MS	1152	T.D. Pointon, 1652
1	MS	1168	P.D. LePell, 1673
1	MS	1186	T.A. Brunner, 1641
1	MS	1186	R.B. Campbell, 1641
1	MS	1186	K.R. Cochrane, 1641
1	MS	1186	C.J. Garasi, 1641
1	MS	1186	T.A. Haill, 1641
1	MS	1186	H.L. Hanshaw, 1641
1	MS	1186	C.A. Jennings, 1641
1	MS	1186	R.W. Lemke, 1641
1	MS	1186	E.P. Yu, 1641
1	MS	1186	P.J. Christenson, 1674
1	MS	1186	T.K. Mattsson, 1641
1	MS	1186	K. Peterson, 1674
1	MS	1186	A.B. Sefkow, 1674
1	MS	1186	S.E. Rosenthal, 1674
1	MS	1186	S.A. Slutz, 1674
1	MS	1186	R.C. Mancini, 1677
1	MS	1191	M.A. Sweeney, 1670
1	MS	1193	D.C. Rovang, 1645
1	MS	1194	J.R. Woodworth, 1671
1	MS	1193	G.R. Bennett, 1672
1	MS	1193	D.L. Hanson, 1673
1	MS	1193	D.B. Sinars, 1673
1	MS	1193	L.A. McPherson, Jr., 1675
1	MS	1186	D.M. Sachs, 1675
1	MS	1192	W.M. White, 1675

1	MS	1193	D.E. Bliss, 1672
1	MS	1194	M.G. Mazarakis, 1671
1	MS	1194	M.E. Savage, 1671
1	MS	1194	K.W. Struve, 1670
1	MS	1196	J.E. Bailey, 1677
1	MS	1196	G.A. Chandler, 1677
1	MS	1196	D.L. Fehl, 1677
1	MS	1196	T.J. Nash, 1677
1	MS	1196	R.E. Olson, 1677
1	MS	1196	G.A. Rochau, 1677
1	MS	1196	C.L. Ruiz, 1677
1	MS	1196	T.W.L. Sanford, 1677
1	MS	0899	Technical Library, 9536 (electronic copy)
1	MS	0123	D. Chavez, LDRD Office, 1011

Sandia National Laboratories